Chapter 25

Trail Blazing: By Solving the Band Gap Problem and the Mystery of First Order Fermi Acceleration in CFLE Theory

25.1. Solving the Band Gap Problem: Why Can Band Gaps Not Accurately Be Calculated?

Electronic band structure is one of the most fundamental properties of a material that plays a crucial role in many important applications, and its accurate description has been a long-standing challenge for the first-principles electronic structure theory. Kohn-Sham Density-functional theory (KS-DFT) within local density or generalized-gradient approximations (LDA/GGA), currently the "standard model" for first-principles computational materials science, suffers from the well-known band gap problem.

In calculating band structure, the local density approximation (LDA) and density functional theory (DFT) are widely popular and do reproduce a lot of the basic physics. Regrettably, without some fine tuning, the LDA and DFT do not generally get the details of the experimental band structure correct, in particular the band gap in semiconductors and insulators is generally found to be too small when compared with experiment.

Predicted value of Silicon Band gap by LDA (Fabien Tran and Peter Blaha at institute of Material Chemistry, Vienna University of technology, Getreidemarkt 9/165-TC, A-1060 Vienna, Austria in physical Review Letters of 05 June 2009) is

$$E_{LDA} = 0.47 \text{ eV} \qquad 25\text{-}1$$

Table 25-1

Theoretical and experimental fundamental band gaps (in eV). The structure is indicated in parenthesis. For comparison, results from the literature which were obtained by other methods are also shown (HSE03, HSE06, G_0W_0, and GW). The experimental values were taken from Refs. [4,7,10,14,18,23–26].

Solid	LDA	MBJLDA	HSE	G_0W_0	GW	Expt.
Ne (A1)	11.42	22.72		19.59[e]	22.1[g]	21.70
Ar (A1)	8.16	13.91	10.34[a]	13.28[e]	14.9[g]	14.20
Kr (A1)	6.76	10.83				11.6
Xe (A1)	5.78	8.52				9.8
C (A4)	4.11	4.93	5.49[b]	5.50[e]	6.18[g]	5.48
Si (A4)	0.47	1.17	1.28[b]	1.12[c]	1.41[g]	1.17
Ge (A4)	0.00	0.85	0.83[c]	0.66[f]	0.95[g]	0.74
LiF (B1)	8.94	12.94		13.27[e]	15.9[g]	14.20
LiCl (B1)	6.06	8.64				9.4
MgO (B1)	4.70	7.17	6.67[b]	7.25[e]	9.16[g]	7.83
ScN (B1)	−0.14	0.90		0.95[f]	1.4[h]	~0.9
MnO (B1)	0.76	2.95	2.8[c]		3.5[i]	3.9 ± 0.4
FeO (B1)	−0.35	1.82	2.2[c]			2.4
NiO (B1)	0.42	4.16	4.2[c]	1.1[f]	4.8[i]	4.0, 4.3
SiC (B3)	1.35	2.28	2.40[b]	2.27[e]	2.88[g]	2.40
BN (B3)	4.39	5.85	5.99[b]	6.10[e]	7.14[g]	~6.25
GaN (B3)	1.63	2.81	3.14[b]	2.80[e]	3.82[g]	3.20
GaAs (B3)	0.30	1.64	1.12[b]	1.30[e]	1.85[g]	1.52
AlP (B3)	1.46	2.32	2.51[b]	2.44[e]	2.90[g]	2.45
ZnS (B3)	1.84	3.66	3.49[b]	3.29[e]	4.15[g]	3.91
CdS (B3)	0.86	2.66	2.25[b]	2.06[e]	2.87[g]	2.42
AlN (B4)	4.17	5.55	5.81[b]	5.83[f]		6.28
ZnO (B4)	0.75	2.68	2.49[d]	2.51[f]	3.8[g]	3.44

[a]HSE06, erratum of Ref. [10].
[b]HSE03, supplementary material of Ref. [4].
[c]HSE03 [26]. [d]HSE06 [27]. [e]Reference [17]. [f]Reference [15].
[g]Reference [18]. [h]Reference [16]. [i]Reference [14].

However, experimental value of Silicon Band gap by $E_g = -\left(\frac{b}{a}\right)e$ (Jeremy J. Low et al at Department of Physics, Millersville University P.O. Box 1002 Millersville, Pennsylvania 17551, USA, in April 16, 2008 of American journal undergraduate research Vol 7, No 1) is

$$E_{EXP} = 1.17eV \qquad 25\text{-}2$$

Table 25-2

	a (K/V)	b (K)	E_g (eV) 273 K to 330 K	E_g (eV) 288 K to 383 K [Ref. 4]	E_g (eV) 300 K [Ref. 6]
MPS2222AG	-462.17 ± 7.95	547.40 ± 4.12	1.20 ± 0.03	1.23	1.12
1N915	-393.54 ± 6.38	454.18 ± 2.39	1.17 ± 0.03		

Linear regression coefficients a and b obtained from measured $T-V$ data, and E_g calculated from them. Last two columns are E_g values at given temperature from Ref. 4 and Ref. 6, for comparison.

This long –standing discrepancy is called the Band gap problem.

In solid-state physics, the electronic band structure (or simply band structure) of a solid describes the range of energies that an electron within the solid may have (called *energy bands*, *allowed bands*, or simply *bands*) and ranges of energy that it may not have (called *band gaps* or *forbidden bands*). Band theory derives these bands and band gaps by examining the allowed quantum mechanical wave functions for an electron in a large, periodic lattice of atoms or molecules. Band theory has been successfully used to explain many physical properties of solids, such as electrical resistivity and optical absorption, and forms the foundation of the understanding of all solid-state devices (transistors, solar cells, etc.).

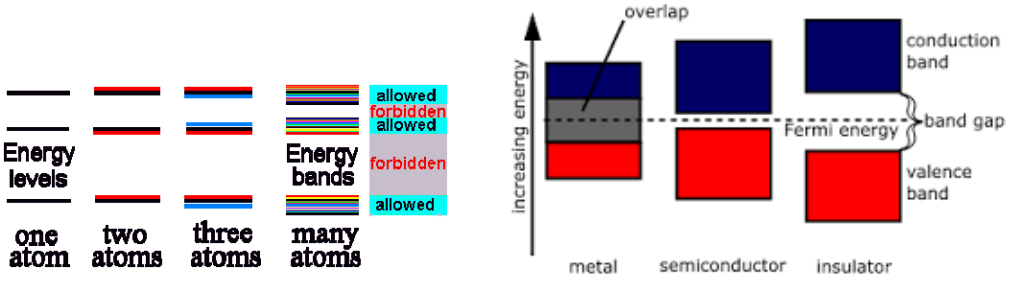

Figure 25-1

It is important to note what has been assumed in order to gain the simplicity of the band theory:

1. *Infinite-size system*: For the bands to be continuous, we must consider a large piece of material. The concept of band structure can be extended to systems which are only "large" along reduced dimensions, such as two-dimensional electron systems.
2. *Homogeneous system*: The notion of a band structure as an intrinsic property of a material assumes that the material is homogeneous in some way. Practically, this means that band structure describes the bulk inside a uniform piece of material.
3. *Non-interactivity*: The band structure describes "single electron states". The existence of these states assumes that the electrons travel in a static potential without dynamically interacting with lattice vibrations, other electrons, photons, etc.

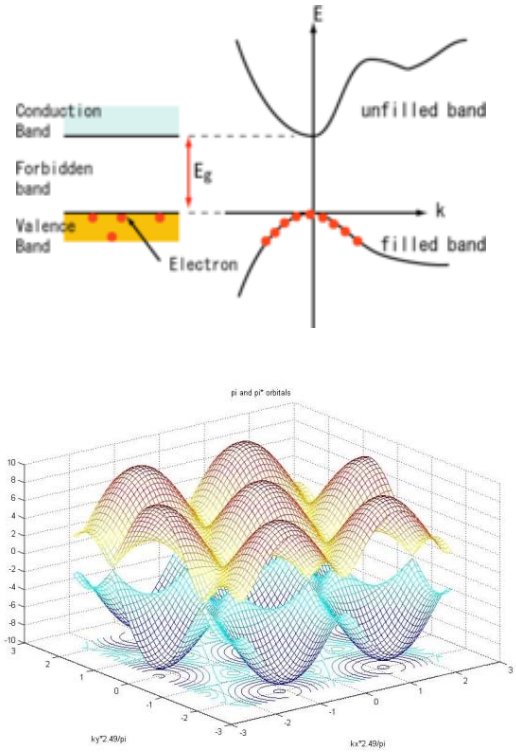

Figure 25-2

The above assumptions are broken in a number of important practical situations, and the use of band structure requires one to keep a close check on the limitations of band theory:

- Inhomogeneities and interfaces: Near surfaces, junctions, and other inhomogeneities, the bulk band structure is disrupted. Not only are there local small-scale disruptions (e.g., surface states or dopant states inside the band gap), but also local charge imbalances. These charge imbalances have electrostatic effects that extend deeply into semiconductors, insulators, and the vacuum (see doping, band bending).
- Along the same lines, most electronic effects (capacitance, electrical conductance, electric-field screening) involve the physics of electrons passing through surfaces and/or near interfaces. The full description of these effects, in a band structure picture, requires at least a rudimentary model of electron-electron interactions (see space charge, band bending).
- Small systems: For systems which are small along every dimension (e.g., a small molecule or a quantum dot), there is no continuous band structure. The crossover between small and large dimensions is the realm of mesoscopic physics.
- Strongly correlated materials (for example, Mott insulators) simply cannot be understood in terms of single-electron states. The electronic band structures of these materials are poorly defined (or at least, not uniquely defined) and may not provide useful information about their physical.

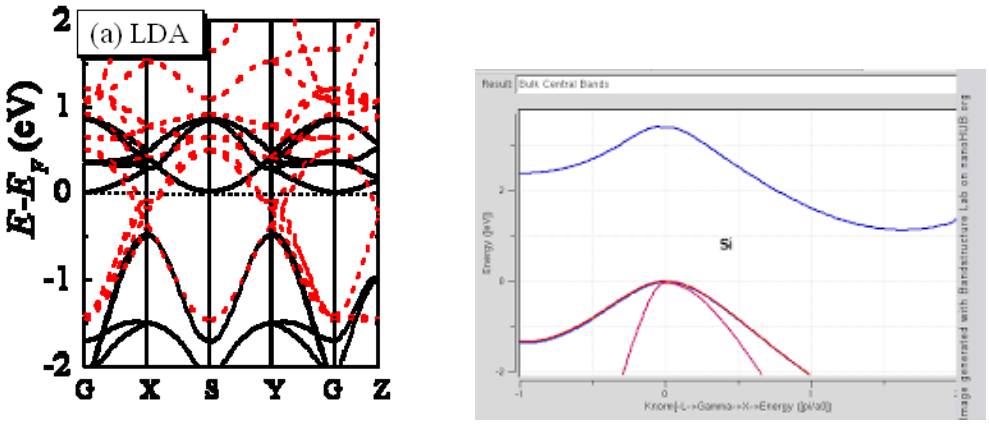

Figure 25-3

Density functional theory (DFT) is a computational quantum mechanical modelling method used in physics, chemistry and materials science to investigate the electronic structure (principally the ground state) of many-body systems, in particular atoms, molecules, and the

condensed phases. Using this theory, the properties of a many-electron system can be determined by using functional,i.e. functions of another function, which in this case is the spatially dependent electron density. Although density functional theory has its conceptual roots in the Thomas–Fermi model, DFT was put on a firm theoretical footing by the two Hohenberg–Kohn theorems (H–K).The original H–K theorems held only for non-degenerate ground states in the absence of a magnetic field, although they have since been generalized to encompass these.
Within the framework of Kohn–Sham DFT (KS DFT), the intractable many-body problem of interacting electrons in a static external potential is reduced to a tractable problem of non-interacting electrons moving in an effective potential. The effective potential includes the external potential and the effects of the Coulomb interactions between the electrons, e.g., the exchange and correlation interactions.

Local-density approximations (LDA) are a class of approximations to the exchange–correlation (XC) energy functional in density functional theory (DFT) that depend solely upon the value of the electronic density at each point in space (and not, for example, derivatives of the density or the Kohn–Sham orbitals). Many approaches can yield local approximations to the XC energy. However, overwhelmingly successful local approximations are those that have been derived from the homogeneous electron gas (HEG) model. In this regard, LDA is generally synonymous with functionals based on the HEG approximation, which are then applied to realistic systems (molecules and solids).

- In general, for a spin-unpolarized system, a local-density approximation for the exchange-correlation energy is written as
- $E_{xc}^{LDA}[\rho] = \int \rho(r)\epsilon_{xc}(\rho)dr$

- where ρ is the electronic density and ε_{xc} is the exchange-correlation energy per particle of a homogeneous electron gas of charge density ρ. The exchange-correlation energy is decomposed into exchange and correlation terms linearly,
- $E_{xc} = E_x + E_c$ so that separate expressions for E_x and E_c are sought. The exchange term takes on a simple analytic form for the HEG. Only limiting expressions for the correlation density are known exactly, leading to numerous different approximations for εc.

In physics, the exchange interaction (with an exchange energy, and exchange term) is a quantum mechanical effect that only occurs between identical particles. Exchange interaction effects were discovered independently by physicists Werner Heisenberg and Paul Dirac in 1926.

Electronic correlation is the interaction between electrons in the electronic structure of a quantum system.

Within the Hartree–Fock method of quantum chemistry, the anti-symmetric wave function is approximated by a single Slater determinant. Exact wave functions, however, cannot generally be expressed as single determinants. The single-determinant approximation does not take into account Coulomb correlation, leading to a total electronic energy different from the exact solution of the non-relativistic Schrödinger equation within the Born–Oppenheimer approximation. Therefore the Hartree–Fock limit is always above this exact energy.

For two independent electrons *a* and *b*,

$$\rho(r_a, r_b) \sim \rho(r_a)\rho(r_b) \qquad 25\text{-}3$$

where $\rho(\mathbf{r}_a,\mathbf{r}_b)$ represents the joint electronic density, or the probability density of finding electron *a* at $\mathbf{r}_a$ and electron *b* at $\mathbf{r}_b$. Within this notation, $\rho\,(\mathbf{r}_a,\mathbf{r}_b)\,d\mathbf{r}_a\,d\mathbf{r}_b$ represents the probability of finding the two electrons in their respective volume elements $d\mathbf{r}_a$ and $d\mathbf{r}_b$.

> If these two electrons are correlated, then the probability of finding electron *a* at a certain position in space depends on the position of electron *b*, and vice versa. In other words, the product of their independent density functions does not adequately describe the real situation. At small distances, the uncorrelated pair density is too large; at large distances, the uncorrelated pair density is too small (i.e. the electrons tend to "avoid each other").

Typically, strongly correlated materials have incompletely filled *d*- or *f*-electron shells with narrow energy bands. One can no longer consider

any electron in the material as being in a "sea" of the averaged motion of the others (also known as mean field theory). Each single electron has a complex influence on its neighbors.

The term strong correlation refers to behavior of electrons in solids that is not well-described (often not even in a qualitatively correct manner) by simple one-electron theories such as the local-density approximation (LDA) of density-functional theory or Hartree–Fock theory. For instance, the seemingly simple material NiO has a partially filled 3*d*-band (the Ni atom has 8 of 10 possible 3*d*-electrons) and therefore would be expected to be a good conductor. However, strong Coulomb repulsion (a correlation effect) between *d*-electrons makes NiO instead a wide-band gap insulator. Thus, strongly correlated materials have electronic structures that are neither simply free-electron-like nor completely ionic, but a mixture of both.

The exchange-correlation potential corresponding to the exchange-correlation energy for a local density approximation is given by

$$v_{xc}^{LDA}(r) = \frac{\delta E^{LDA}}{\delta \rho(r)} = \epsilon_{xc}\big(\rho(r)\big) + \rho(r)\frac{\partial \epsilon_{xc}(\rho(r)}{\partial \rho(r)} \qquad 25\text{-}4$$

In finite systems, the LDA potential decays asymptotically with an exponential form. This is in error; the true exchange-correlation potential decays much slower in a Coulombic manner. The artificially rapid decay manifests itself in the number of Kohn–Sham orbitals the potential can bind (that is, how many orbitals have energy less than zero). The LDA potential cannot support a Rydberg series and those states it does bind are too high in energy. These results in the HOMO energy being too high in energy, so that any predictions for the ionization potential based on Koopman's theorem are poor. Further, the LDA provides a poor description of electron-rich species such as anions where it is often unable to bind an additional electron, erroneously predicating species to be unstable.

a general exchange functional for an arbitrary electron–electron interaction w_{ee}(r) is

$$E_X[n; w_{ee}] = \langle \Phi[n] | \widehat{w_{ee}} | \Phi[n] \rangle - E_H[n; w_{ee}] \qquad 25\text{-}5$$

general correlation functional associated to w_{ee}(r) writes

$$E_c[n; w_{ee}] = \min_{\Psi \to n} \langle \Psi \left| \hat{T} + \widehat{w_{ee}} \right| \Psi \rangle - \langle \Phi[n] \left| \hat{T} + \widehat{w_{ee}} \right| \Phi[n] \rangle \quad 25\text{-}6$$

the following decomposition of the Coulomb electron–electron interaction $w_{ee}^{coul}(r) = \frac{1}{r}$ is

$$w_{ee}^{coul}(r) = w_{ee}^{lr,\mu}(r) + w_{ee}^{sr,\mu}(r) \quad 25\text{-}7$$

The Coulombic exchange functional is consequently decomposed as

$$E_X^{coul}[\mathrm{n}] = E_X^{lr,\mu}[\mathrm{n}] + E_X^{sr,\mu}[\mathrm{n}] \quad 25\text{-}8$$

However, Coulombic correlation functional is

$$E_c^{coul}[\mathrm{n}] \neq E_c^{lr,\mu}[\mathrm{n}] + E_c^{sr,\mu}[\mathrm{n}] \quad 25\text{-}9$$

Instead, one can write $E_c^{coul}[\mathrm{n}]$ exactly as

$$E_c^{coul}[\mathrm{n}] = E_c^{lr,\mu}[\mathrm{n}] + E_c^{sr,\mu}[\mathrm{n}] + E_c^{lr-sr,\mu}[\mathrm{n}] \quad 25\text{-}10$$

By associating the mixed term $E_c[n; w_{ee}]$ to either the long or the short-range part of the correlation energy, one obtains two possible long-range/short-range decompositions.

The first one is

$$E_c^{coul}[\mathrm{n}] = E_c^{lr,\mu}[\mathrm{n}] + E_c^{-sr,\mu}[\mathrm{n}] \quad 25\text{-}11$$

The second one is

$$E_c^{coul}[\mathrm{n}] = E_c^{-lr,\mu}[\mathrm{n}] + E_c^{sr,\mu}[\mathrm{n}] \quad 25\text{-}12$$

the second-order Coulombic correlation energy is

$$E_c^{coul,(2)} = \sum_i \frac{\left| \langle \Phi \left| \hat{w}_{ee}^{coul} - \hat{\mathrm{V}}_{Hx}^{coul} \right| \Phi_\mathrm{i} \rangle \right|^2}{E_s - E_{s,i}} \quad 25\text{-}13$$

The second-order long-range correlation energy writes

$$E_c^{1r,\mu,(2)} = \sum_i \frac{\left| \langle \Phi \left| \hat{w}_{ee}^{lr,\mu} - \hat{\mathrm{V}}_{Hx}^{lr,\mu} \right| \Phi_\mathrm{i} \rangle \right|^2}{E_s - E_{s,i}} \quad 25\text{-}14$$

the second-order short-range correlation energy writes

$$E_c^{sr,\mu,(2)} = \sum_i \frac{|\langle\Phi|\hat{w}_{ee}^{sr,\mu} - \hat{V}_{Hx}^{sr,\mu}|\Phi_i\rangle|^2}{E_s - E_{s,i}} \quad 25\text{-}15$$

Finally, the second-order mixed long-range/short-range correlation functional is

$$E_c^{lr-sr,\mu,(2)} = 2\sum_i \frac{\left|\left\langle\Phi\right| \hat{w}_{ee}^{lr,\mu} - \hat{V}_{Hx}^{lr,\mu}\left|\phi_i\right\rangle\langle\phi_i|\hat{w}_{ee}^{sr,\mu} - \hat{V}_{Hx}^{sr,\mu}|\Phi_i\rangle\right|}{E_s - E_{s,i}} \quad 25\text{-}16$$

The short range exchange LDA functional associated to $E_X^{sr,\mu}[n]$ writes

$$E_{X,LDA}^{sr,\mu}[n] = \int n(r)\varepsilon_{X,unif}^{sr,\mu}\big(n(r)\big)dr \quad 25\text{-}17$$

the short range correlation LDA functional for $E_c^{sr,\mu}[n]$ is

$$E_{c,LDA}^{-sr,\mu}[n] = \int n(r)\varepsilon_{c,unif}^{-sr,\mu}\big(n(r)\big)dr \quad 25\text{-}18$$

The LDA for $E_c^{sr,\mu}[n]$ writes

$$E_{c,LDA}^{sr,\mu}[n] = \int n(r)\varepsilon_{c,unif}^{sr,\mu}\big(n(r)\big)dr \quad 25\text{-}19$$

Here important point is that we cannot find any physical, mathematical discrepancies of DFT and LDA.

In quantum chemistry and molecular physics, the Born–Oppenheimer (BO) approximation that was proposed in 1927 in the early period of quantum mechanics by Born and Oppenheimer and is still indispensable in quantum chemistry is the assumption that the motion of atomic nuclei and electrons in a molecule can be separated. The approach is named after Max Born and J. Robert Oppenheimer. In mathematical terms, it allows the wave function of a molecule to be broken into its electronic and nuclear (vibrational, rotational) components.

- $\Psi_{total} = \psi_{electrinic} \times \psi_{nuclear}$
- Computation of the energy and the wave function of an average-size molecule is simplified by the approximation.

The Hartree–Fock method makes five major simplifications in order to deal with this task:

- The Born–Oppenheimer approximation is inherently assumed. The full molecular wave function is actually a function of the coordinates of each of the nuclei, in addition to those of the electrons.
- Typically, relativistic effects are completely neglected. The momentum operator is assumed to be completely non-relativistic.
- The variational solution is assumed to be a linear combination of a finite number of basic functions, which are usually (but not always) chosen to be orthogonal. The finite basis set is assumed to be approximately complete.
- Each energy eigenfunction is assumed to be describable by a single Slater determinant, an antisymmetrized product of one-electron wave functions (i.e., orbitals).
- The mean field approximation is implied. Effects arising from deviations from this assumption, known as electron correlation, are completely neglected for the electrons of opposite spin, but are taken into account for electrons of parallel spin.(Electron correlation should not be confused with electron exchange, which is fully accounted for in the Hartree–Fock method.)

The Hamiltonian for the nuclei-electron systems can write

$$H = -\frac{1}{2}\sum_A \frac{\nabla_A^2}{M_A} + \frac{1}{2}\sum_{A\neq B} \frac{Z_A Z_B}{R_{AB}} - \sum_{i,A} \frac{Z_A}{r_{iA}} - \frac{1}{2}\sum_i \frac{\nabla_i^2}{m_e} + \sum_{i,j} \frac{1}{r_{ij}} \qquad 25\text{-}20$$

First part of Born-Oppenheimer approximation (BOA): Write the total wave function as a product of a nuclear part $v\,(R)$ and an electronic part $\Psi(\{r\};\,\{R\})$, where the semicolon represents the fact that the nuclear coordinates are static parameters.

$$\Phi(\{r\};\,\{R\}) = \nu\{R\}\Psi(\{r\};\,\{R\}) \qquad 25\text{-}21$$

Second part of Born-Oppenheimer approximation (BOA): determine $\Psi(\{r\};\,\{R\})$ from the part of the Hamiltonian with static nuclei and ignore cross terms of the nuclear kinetic operator with the electronic part of the wave function.

$$H|\phi(\{r\};\,\{R\})\rangle$$

$$= (\sum_A \frac{\nabla_A^2}{M_A} + \frac{1}{2}\sum_{A\neq B} \frac{Z_A Z_B}{R_{AB}} + H_{el}(r;R))|\Psi(\{r\};\{R\})\rangle|v\{R\}\rangle$$

$$= [H_{el}(r;R)|\Psi(\{r\};\{R\})\rangle(\sum_A -\frac{1}{2}\frac{\nabla_A^2}{M_A} + \frac{1}{2}\sum_{A\neq B}\frac{Z_A Z_B}{R_{AB}})]\,|v\{R\}\rangle \qquad 25\text{-}22$$

$$H_{el} = \sum_{i,A}\frac{Z_A}{r_{iA}} - \frac{1}{2}\sum_i \frac{\nabla_i^2}{m_e} + \sum_{i,j}\frac{1}{r_{ij}} \qquad 25\text{-}23$$

The simplest assumption is that the wave function is composed of a product of one electron wave functions:

$$\Psi(\{r\}) = |x_1(r1)x_{2(r2)}x_3(r3)\cdots\rangle \qquad 25\text{-}24$$

This is known as a Hartree product.

Therefore the simplest physical wave function can have form as:

$$\Psi(\{r\}) = \sqrt{\frac{1}{N!}}\ \sum_n^{n=N!}((-1)^{P_n}P_n(\,x_1(r1)x_{2(r2)}x_3(r3)\cdots)) \qquad 25\text{-}25$$

This Hartree Fock method (HFM) consists in finding the variational value of the electronic energy for such a Wave function.

The Born-Oppenheimer approximation is one of the best approximations in chemical physics in the sense that it proves to be a valid approximation in most situations. In the Born-Oppenheimer approximation and The Hartree–Fock method we cannot find any physical and mathematical defects.

In physics and quantum chemistry, specifically density functional theory, the Kohn–Sham equation is the Schrödinger equation of a fictitious system (the "Kohn–Sham system") of non-interacting particles (typically electrons) that generate the same density as any given system of interacting particles. The Kohn–Sham equation(KSE) is defined by a local effective (fictitious) external potential in which the non-interacting particles move, typically denoted as v_s(r) or v_{eff}(r), called the Kohn–Sham potential. As the particles in the Kohn–Sham system are non-interacting fermions, the Kohn–Sham wave function is a single Slater determinant constructed from a set of orbitals that are the lowest energy solutions to

$$\left(-\frac{\hbar^2}{2m}\nabla^2 + v_{eff}(r)\right)\phi_i(r) = \varepsilon_i\phi_i(r) \qquad 25\text{-}26$$

This eigenvalue equation is the typical representation of the Kohn–Sham equations. Here, ε_i is the orbital energy of the corresponding Kohn–Sham orbital, φ_i, and the density for an N-particle system is

$$\rho(r) = \sum_i^N |\phi_i(r)|^2 \qquad 25\text{-}27$$

Here, also in Kohn-Sham equation we cannot find any physical, mathematical incongruity.

Such correct results of DFT, LDA, BOA, HFM and KSE mean that DFT, LDA, BOA, HFM and KSE cannot explain the band gap problem.

However, CFLE theory can explain directly this band gap problem by correspondence number $C_c = 1.5$ from energy of accelerating universe (cf. §24).

This means that total mass of solid system as part of universe must be correlated with electronic correlate energy for band gap.

Because correspondence number $C_c = 1.5$ is ratio between mass of accelerating universe and electric charge of different part of universe, ratio between gravitational potential and electronic potential for correlation potential of density functional is

$$C_c^2 = (1.5)^2 = 2.25 \qquad 25\text{-}28$$

Related difference of gravitational permittivity of air is

$$Q_g = (0.016774 \times 2 \times 1.5) = 0.050322$$

$$x_{gair} = 1.050322$$

$$x_{gair}^2 = 1.103176 \qquad 25\text{-}29$$

Therefore, now real band gap of solid of silicon by CFLE theory should be

$$E_{LDA} = (0.47\ eV)(2.25)(1.103176) = 1.166\ eV \qquad 25\text{-}30$$

Experimental value is

$$E_{LDA} = 1.17 \text{ eV} \qquad 25\text{-}2$$

This agreement say us that effect of accelerating universe influence not only to galaxy clusters, galaxies, stars and its planets as huge macro gravitational system but also to molecular and small solid as P-N semiconductor as micro gravitational system.

In CFLE Theory such mysterious band gap energy discrepancy is not strange phenomenon, but also universal phenomena at planet Earth (cf.§5.3 ratio between earth mass and correspondence electric charge), at Solar system (cf.§9.1 ratio between quantized gravitational radius of the solar system and quantized electric radius) at theoretical deduction of gravitational constant from electrical constant (cf.§10.5 ratio between electrical constant and gravitational constant) and quantisation of electric charge (cf.§18,Eq.18.3.32) etc…

25.2. Solving Semiconductor Nanocrystals Problem: What Is the Cause of the Nonparabolicity of the Energy-Size Dependence for the Lowest Optical Absorption Transition of Quantum Dots?

Such mysterious effect from accelerating universe really can be influence to size of semiconductor nanocrystal too as serious problem of What is the cause of the nonparabolicity of the energy-size dependence for the lowest optical absorption transition of quantum dots(QD) as semiconductor nanocrystals as Figure 25-6 ?

A nanocrystal is a material particle having at least one dimension smaller than 100 nanometres (a nanoparticle) and composed of atoms in either a single- or poly-crystalline arrangement.

The size of nanocrystals distinguishes them from larger crystals. For example, silicon nanocrystals can provide efficient light emission while bulk silicon does not and may be used for memory components.

Quantum dots (QD) are semiconductor devices that tightly confine electrons or holes in all three spatial dimensions. In a semiconductor crystallite whose size is smaller than twice the size of its exciton Bohr radius, the excitons are squeezed, leading to quantum confinement. They can be made via several possible routes including colloidal

synthesis, plasma synthesis, or mechanical fabrication. The term "quantum dot" was coined by Mark Reed in 1988. However, they were first discovered in a glass matrix by Alexey Ekimov in 1981 and in colloidal solutions by Louis E. Brus in 1985.

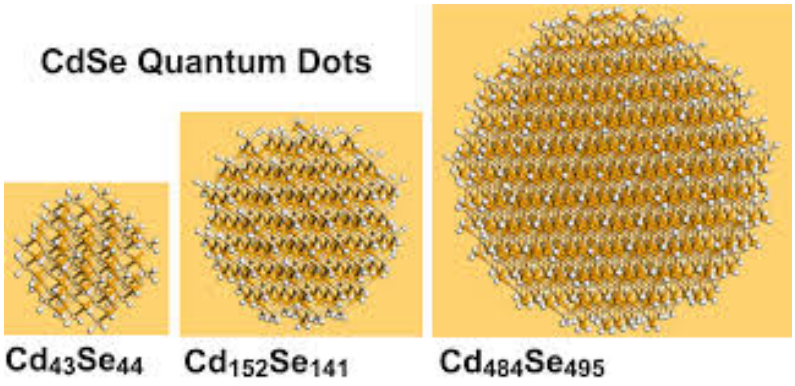

Figure 25-4

The electronic properties of the quantum dots fall between those of bulk semiconductors and those of discrete molecules of comparable size, and optoelectronic properties such as band gap, can be tuned as a function of particle size and shape for a given composition. For example, the photoluminescence of a QD can be manipulated to specific wavelengths by controlling particle diameter.

Larger QDs (radius of 5-6 nm, for example) emit longer wavelengths resulting in emission colors such as orange or red. Smaller QDs (radius of 2-3 nm, for example) emit shorter wavelengths resulting in colors like blue and green, although the specific colors and sizes vary depending on the exact composition of the QD. Dots may also be made from ternary compounds such as cadmium selenide sulfide.

These quantum dots can contain as few as 100 to 100,000 atoms within the quantum dot volume, with a diameter of ~ 10 to 50 atoms. This corresponds to about 2 to 10 nanometers, and at 10 nm in diameter, nearly 3 million quantum dots could be lined up end to end and fit within the width of a human thumb. Large batches of quantum dots may be synthesized via colloidal synthesis.

An exciton is a bound state of an electron and an electron hole which are attracted to each other by the electrostatic Coulomb force.

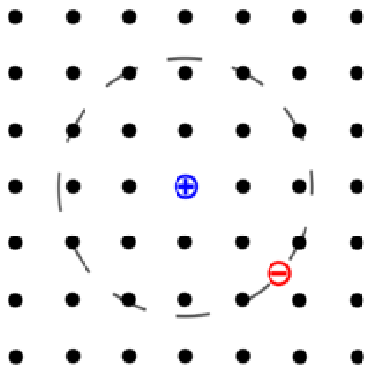

Figure 25-5

It is an electrically neutral quasiparticle that exists in insulators, semiconductors and in some liquids. The exciton is regarded as an elementary excitation of condensed matter that can transport energy without transporting net electric charge.

An exciton can form when a photon is absorbed by a semiconductor. This excites an electron from the valence band into the conduction band.

Excitons are the main mechanism for light emission in semiconductors at low temperature (when the characteristic thermal energy kT is less than the exciton binding energy), replacing the free electron-hole recombination at higher temperatures.

The existence of exciton states may be inferred from the absorption of light associated with their excitation

The mystery of this nonparabolicity of the energy-size dependence for the lowest optical absorption transition of quantum dots as semiconductor nanocrystals as Figure 25-6 is discrepancy between theory of the effective mass model and observation.

Calculating quantum dot transitions as a function of size using the effective mass theory, which includes valence-band mixing and uses the Kane model to incorporate the nonparabolicity of the conduction band.

Electron eigenvalues are evaluated by numerically solving the boundary condition.

$$[1+2f+\frac{E_p}{3}(\frac{2}{E+\frac{E_g}{2}}+\frac{1}{E+\frac{E}{2}+\Delta})]$$

$$\times\frac{\partial}{\partial r}\ln[j_l\,(k_s r]\,|_{r=a}=\frac{\partial}{\partial r}\ln[K_l'(k_m r)]|_{r=a} \qquad 25\text{-}31$$

which matches the semiconductor conduction band with the surrounding matrix. A simple free-electron form is assumed for the matrix, which in our samples is an organic solvent.

Here a is the quantum dot radius, E_g is the semiconductor band gap, Δ is the spin-orbit coupling,$j_{l(z)}$ is the l th-order spherical Bessel function, and

$$K_l'(z)=(\frac{\pi}{2z})^{1/2}K_{l+1/2(z)} \qquad 25\text{-}32$$

With $K_{l+1/2(z)}$the modified Bessel function. The energy of the electron level (E) is measured from midgap. The wave vectors in the semiconductor (k_s) and matrix (k_m) are given by

$$k_s^2=\frac{2m_o}{\hbar^2}[E-\frac{E_g}{2}][1+2f+\frac{E_p}{3}(\frac{2}{E+\frac{E_g}{2}}+\frac{1}{E+\frac{E}{2}+\Delta})]^{-1} \qquad 25\text{-}33$$

and

$$k_m^2=\frac{2m_o}{\hbar^2}\left[E-V_e-\frac{E_g}{2}\right] \qquad 25\text{-}34$$

$$\Delta=0.42eV,\ E_g=1.839eV,\ m_e=0.11m_o,\ E_p=17.5\text{ eV} \qquad 25\text{-}35$$

where m_o is the free-electron mass. In these equations E_p and f are Kane model parameters which describe the conduction-band curvature.$E_p(f)$ accounts for the influence of the valence band (higher bands) on the conduction band. Since E_p and f are related to m_e , the effective mass of the electron at the bottom of the conduction band, the electron levels are described by the parameters Δ,E_g ,V_e,m_e, and E_p.

From Eq.25-31 to 25-35 we cannot find any theoretical and physical defects.

However, obtained curve by theory with effective mass calculations is different by experiment with PLE data as Figure 25-6 .

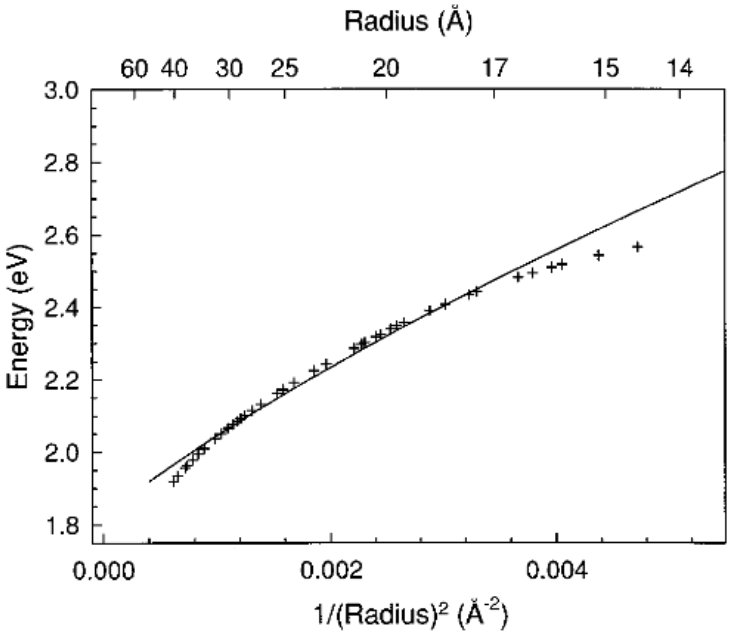

Energy of the first excited state $(1S_{3/2}1S_e)$ in CDSe vs 1/radius^2.
The curve (solid line) obtained from theory is compared with PLE data (crosses). Physical review B Vol 52,No24,15.June 1996
D.J. Norris and M.G. Bawendi at Massachusetts Institute of Technology

Figure 25-6

This quantitative differences between experiment and theory drive us what the cause of the nonparabolicity of the energy-size dependence for the lowest optical absorption transition of quantum dots is.

To explain about cause of the nonparabolicity of the energy-size dependence for the lowest optical absorption transition of quantum dots as semiconductor nanocrystals in Figure 25-6 by CFLE theory is very simple.

Because typically excitons are observed just below the band gap as Figure 25-7, this nonparabolicity must be correlated with extra band gap energy of Eq. 25-30 and Eq.25-31 by correspondence number$C_c = 1.5$ from accelerating universe.

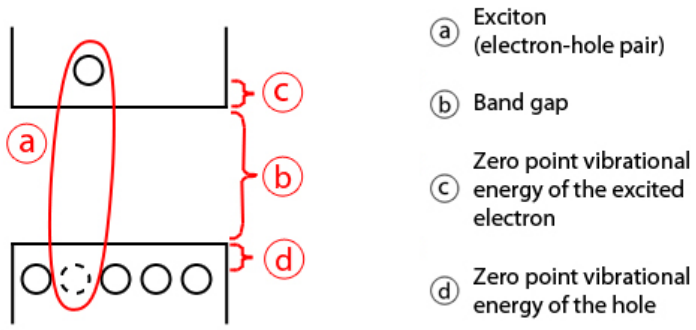

Figure 25-7

Furthermore, the influence of nonparabolicity on the subband structure in a quantum well can be expressed in terms of the perpendicular mass, which is relevant for the determination of confinement energies, and the parallel mass, which gives the curvature of E at the bottom of a subband. Scientists derive approximate expressions for these masses in the form of explicit functions of the confinement energy, which is experimentally accessible.

Here, important point is that the enhancement of the parallel mass relative to the bulk mass is found to be 2–3 times stronger than that of the perpendicular mass. It is shown that the boundary conditions need to be modified in the nonparabolic case.

Cause of this factor of $2 \sim 3$ in quantum well indicate too correspondence number $C_c = 1.5$ from accelerating universe as same cause of band gap energy and related nonparabolicity of quantum dots.

For energy $C_c = 1.5$ is calculated

$$C_c^2 = (1.5)^2 = 2.25 \qquad 25\text{-}28$$

Therefore, diagram of this nonparabolicity of the energy-size dependence for the lowest optical absorption transition of quantum dots and recession velocity of accelerating universe should be essentially almost similar as Figure 25-8.

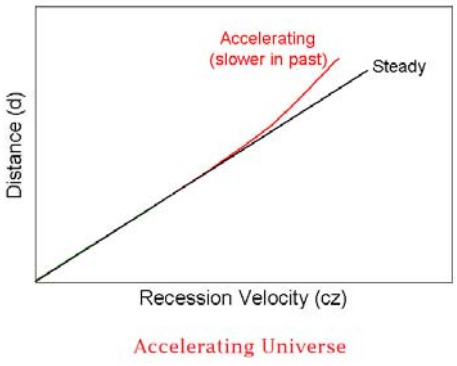

A

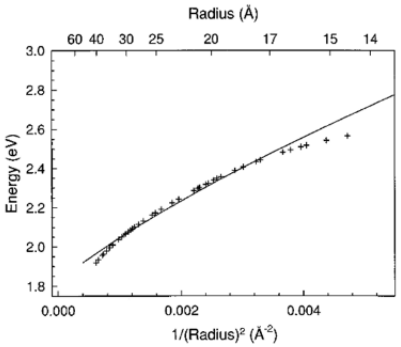

Energy of the first excited state ($1S_{3/2}1S_e$) in CDSe vs 1/radius^2.
The curve (solid line) obtained from theory is compared with PLE data (crosses). Physical review B Vol 52,No24,15 June 1996
D.J. Norris and M.G. Bawendi at Massachusetts Institute of Technology

B

Figure 25-8

This means that mysterious effect between electric charge and gravitational mass by accelerating universe is influenced not only to macroscopic astronomical scale: cosmic coincident problem (cf.§24),dark energy microscopic astronomical scale: Earth's magnetic field generation by mass, radius of solar system … (cf.§5, §9,§11,§13) but also to quantum mechanical scale: band gab problem …(cf.§TB25) and nucleon scale: semi empirical mass formula(cf.§14).

25.3. Solving Dimensionless Physical Constants Problem: Why the Values of the Dimensionless Physical Constants Cannot Be Calculated at the Present Time, and Why They Are Determined Only by Physical Measurement?

Because in CFLE theory fine structure constant $\alpha_e = \frac{1}{137.035999} = \frac{1}{g_8 \times g_8 \times C_{c1.5} \times C_{c1.5}}$ of Eq. 6-4-3-2 is dimensionless electric coupling constant and strong coupling constant$\alpha_s = 1$ is, such universal effect from accelerating universe can be reached to size of subnuclear scale. Good example is factor of 2 of asymmetric term a_A by Pauli principle in semi empirical mass formula from $C_c^2 = (1.5)^2 = 2.25$ in §14.3. A dimensionless physical constant, sometimes called a fundamental physical constant, is a physical constant that is dimensionless.

The numerical values of dimensionless physical constants are independent of the units used. These constants cannot be eliminated by any choice of a system of units. Such constants include:

- α, the fine structure constant, the coupling constant for the electromagnetic interaction (≈1/137.036). Also the square of the electron charge, expressed in Planck units, which defines the scale of charge of elementary particles with charge.
- μ or β, the proton-to-electron mass ratio, the rest mass of the proton divided by that of the electron (≈1836.15). More generally, the ratio of the rest masses of any pair of elementary particles.
- α_s, the coupling constant for the strong force (≈1)
- α_G, the gravitational coupling constant (≈10^{-45}) which is the square of the electron mass, expressed in Planck units. This defines the scale of the masses of elementary particles and has also been used to express the relative strength of gravitation.

Unlike mathematical constants, the values of the dimensionless fundamental physical constants cannot be calculated according to modern physics. At the present time, under the modern physics they are determined only by physical measurement.

This problem become one of the important unsolved problems of modern physics as what the minimum number of dimensionless physical constants is from which all other dimensionless physical constants can be derived.

However, because metaphysical curve able space-time continuum that was introduced by H. Minkowski and A. Einstein does not exist in CFLE theory, dimensionless constant can be calculable as degree of curve of force lines by moving force line elements(cf.§4,§6,§7).

Essence of the proton-to-electron rest mass ratio is too ratio between degree of curve of force line of rest proton and rest electron as general relativity of CFLE theory

$$R_{\frac{p}{e}} = \frac{g_{sp} \times g_{ep} \times g_{wp} \times g_{gp}}{g_{se} \times g_{ee} \times g_{we} \times g_{ge}} = \frac{6.546 \times 6.546 \times 86.546 \times 6.546}{1 \times 1 \times 1 \times 1}$$

$$= 1836.15 \qquad 25\text{-}36$$

where g_{sp} is curve of strong force line of proton, g_{ep} is curve of electric force line, g_{wp} is curve of weak force line, g_{ge} is curve of gravitational force line and others are flat of all kind of force lines of electron.

Because present physics doesn't have calculable general relativity, present physics cannot calculate dimension less physical constant that is occurred by degree of curve of force lines.

25.4. Solving the Injection Problem

Fermi acceleration is thought to be the primary mechanism that accelerates astrophysical particles to high energy. However, it is unclear what mechanism causes those particles to initially have energies high enough for Fermi acceleration to work on them.

By this degree of curve of force line as result of general relativity of CFLE theory, the Mystery of first order Fermi acceleration (sometimes called the injection problem) can be solved perfectly as below.

Fermi acceleration, first suggested by Enrico Fermi in 1949, to explain the explain the origin of cosmic rays, sometimes referred to as diffusive shock acceleration (a subclass of Fermi acceleration), is the acceleration that charged particles undergo when being repeatedly reflected, usually by a magnetic mirror. This is thought to be the primary mechanism by which particles gain non thermal energies in astrophysical shock waves. It plays a very important role in many astrophysical models, mainly of shocks including supernova remnants (SNRs) and active galactic nuclei (AGN). There are two types of Fermi acceleration. The first-order Fermi acceleration is that the mean energy gain depends only linearly on the shock velocity. The second-order Fermi acceleration is that the probability of a head-on collision is greater than a head-tail collision, so particles would, on average, be accelerated. The mean energy gain per bounce depends on the mirror velocity squared.

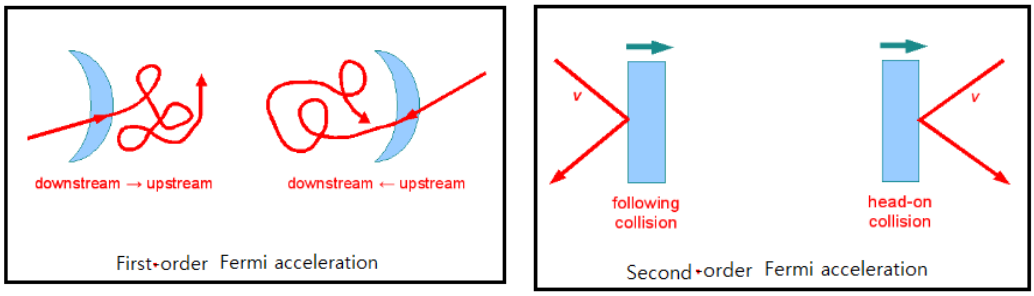

Figure 25-9

Fermi acceleration at (unmodified) nonrelativistic shocks is known to produce power law particle spectra

$\mathbf{N(\gamma) \propto \gamma^{-s}}$ **,** which are essentially independent of the microphysics involved and only dependent on the shock compression ratio when $1 < \rho < 4$

$$\rho = \frac{u_d}{u_u} \qquad 25\text{-}37$$

Spectral index is

$$s = \frac{\rho+2}{\rho-1} \qquad 25\text{-}38$$

For strong shocks ($\rho = 4$ in the test particle limit) the famous $s = 2$ result is obtained.

However, incorporation of non-linear effects (e.g., strong shock modification) usually suggests values

$s < 2$ at high energies (Berezhko and Ellison, 1999).

On the other hand, incorporation of anomalous (non-diffusive) transport properties associated with the wandering of magnetic field lines, may efficiently reduce cross-field propagation and thus allow values up to $s > 2.5$ (Kirk et al., 1996) as Figure 25-10.

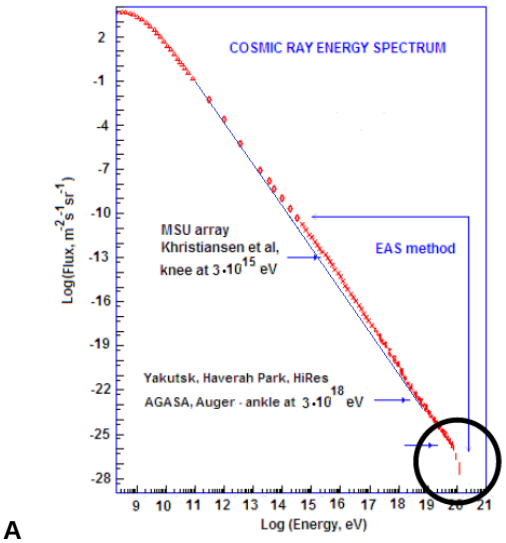

A

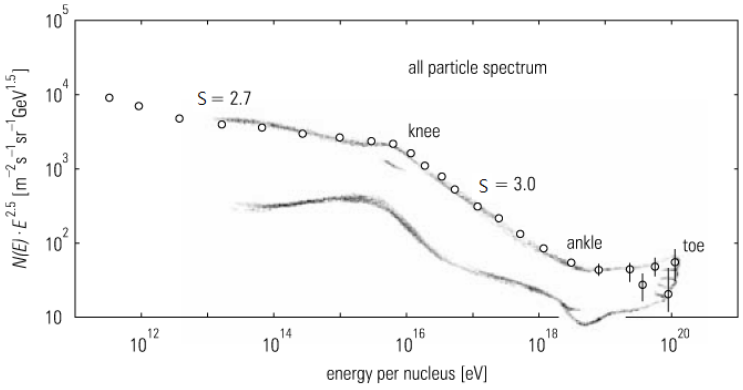

B

The energy spectrum of the cosmic radiation calculated (blue line) by the Theory of Constant Indices (TCI) in 2008 along with the data points of the Tibet, Tunka, Fly's Eye, Haverah Park and Auger experiments, arbitrarily selected out of many others. The agreement in whole range $10^{12} - 5 \times 10^{19}$eV is unparalleled by any other attempts to calculate the spectrum. The energy range of applicability of the TCI is dictated by the relationship between the knee and the ankle discovered in 2006 with an upper energy extreme of 5×10^{19} eV . Precise measurements of Auger and TA experiments (2011) indicate that the galactic spectrum of the cosmic radiation has a break at 2×10^{19} eV. The FIGA effect is probably at the origin of the rapid descend in the measured spectrum above 2×10^{19} eV, which predicts only heavy and very heavy ions from $2\times 10^{19} - 2 \times 10^{20}$ eV.

Figure 25-10

Furthermore, to undergo efficient first-order Fermi acceleration at non-relativistic shocks electrons already have to be preaccelerated up to seed Lorentz factors as ion cyclotron resonance condition over

$$\gamma_e > \frac{m_p}{m_e}\left(\frac{V_A}{c}\right) \qquad 25\text{-}39$$

This power law index problem is called cosmic ray knee problem.

This Mystery of first-order Fermi acceleration called the Injection problem is become great problem as what mechanism causes those particles to initially have energies high enough for Fermi acceleration to work on them.

However, because CFLE theory can calculate total effect of curve of all force lines, CFLE theory can predict the origin of such pre acceleration.

The Lorentz factor of non-relativistic shock of first order Fermi acceleration of supernovae remnants as Preacceleration by curved gravitational field of supernova is

$$\gamma_{SNr}=g^4C_c^4 = (6.546)^4(1.5)^4 = 1836 \times 5.1 = 9296 \approx 10^4 \qquad 25\text{-}40$$

This factor is called supernovae curvature factor

The Lorentz factor of non-relativistic shock of first order Fermi acceleration of active galactic nuclei as Preacceleration by curved gravitational field of AGN is

$$\gamma_{AGN} =g^5C_c^5 = (6.546)^5(1.5)^5$$

$$= 12018 \times 7.6 = 91262 \approx 10^5 \qquad 25\text{-}41$$

This factor is called galactic curvature factor

The Lorentz factor of non-relativistic shock of first order Fermi acceleration of active cosmotomic nucleus (ACN) as Preacceleration by curved gravitational field of ACN is

$$\gamma_{ACN} =g^6C_c^6 = (6.546)^6(1.5)^6$$

$$= 78678 \times 11 = 865458 \approx 10^6 \qquad 25\text{-}42$$

This factor is called cosmotomic curvature factor.

Here, between general use of “cosmic” and “cosmic” of curvature by cosmic nucleus to distinguish is used “cosmotomic” for cosmic nucleus.

However, calculation of Lorentz factor of relativistic shock of first order Fermi acceleration can be calculated by dimensionless charge interval constant $\mathrm{N} = 1.190208 \times 10^7$(cf. §3).

The energy of first order Fermi acceleration of supernova remnants by maximum Lorentz factor of relativistic shock for an electron is

$$E_{\gamma SNr} = (1.190208 \times 10^7)(1.5)(347)(13.6eV)$$

$$= 8.42 \times 10^{10} eV \qquad 25\text{-}43$$

where 1.5 is correspondence number (cf. §24), 347 is stellar mass number (cf. §8), 13.6 eV is electron energy of ground state in hydrogen atom.

This energy is called Fermi energy of supernovae electron.

The energy of first order Fermi acceleration of active galactic nuclei by maximum Lorentz factor of relativistic shock for an electron is

$$E_{\gamma AGN} = (8.42 \times 10^{10} eV)(1.190208 \times 10^7)(1.5)(2027)$$

$$= 3.05 \times 10^{21} eV \qquad 25\text{-}44$$

where 2027 is galaxy mass number(cf. §11)

This energy is called Fermi energy of galactic electron.

Because modern mechanic doesn't have calculable general relativity, preacceleration by curve of force line cannot be explained.

25.5. Solving the Cosmic Ray Paradox: Why Is It That Some Cosmic Rays Appear to Possess Energies That Are Theoretically Too High? Why Is It that (Apparently) Some Cosmic Rays Emitted by Distant Sources Have Energies Above the Greisen–Zatsepin–Kuzmin Limit?

Famous energy of "Oh my god" particle is $E = 3.12 \times 10^{20} eV$ and energy of GZK limit is $E = 5 \times 10^{19} eV$.

Because for GZK limit to calculate cannot be used theory of general relativity, right energy limit to obtain factor of curve of force lines must

be added as dark matter $g^2 = (4.663)^2$ from ordinary matter 0.046%(cf.§7,§24), correspondence number $C_c^2 = (1.5)^2$ from accelerating universe(cf.§24), keplerian missing factor $f_k = 1.202$ (cf.§11) and factor of gravitational permittivity $(x_g)^2 = (1.020353)^2$ of air by difference of electrical permittivity of air $x_e = 1.004712$(cf.§10).

Total missing factor by curvature of force lines is

$f_{missing} = (4.663)^2(1.5)^2(1.202)\,(1.020353)^2 = 61.22$

Therefore, right energy limit should be

$E_{right} = (5 \times 10^{19} eV)(61) = 3.05 \times 10^{21} eV$

Fermi energy of galactic electron of Eq.25-44 is

$$E_{\gamma AGN} = (8.42 \times 10^{10} eV)(1.190208 \times 10^{7})(1.5)(2027)$$

$$= 3.05 \times 10^{21} eV \qquad 25\text{-}44$$

where $x_g = 1.020353$ is obtained from gravitational permittivity of air at $g_{1.5} = 1.025161$(cf.§10) by $C_c = 1.5$ during electrical permittivity of air change atg $= 8$.

$Q = 0.000589 \times 8 = 0.004712$, $x_e = 1.004712$

net change of gravitational permittivity of air is

$$d = \frac{1.025161}{1.004712} = 1.020353$$

Therefore, we can conclude that GZK limit is wrong limit.

The energy of first order Fermi acceleration of active cosmotomic nucleus by maximum Lorentz factor of relativistic shock for an electron is

$$E_{\gamma ACN} = (3.05 \times 10^{21} eV)(1.190208 \times 10^{7})(1.5)(1.38 \times 10^{4})$$

$$= 7.51 \times 10^{32} eV \qquad 25\text{-}45$$

where 1.38×10^4 is cosmotomic mass number (cf. §13)

This energy is called Fermi energy of cosmotomic electron.

Famous Planck mass is bar mass of electric seed of usual electron (cf. §3.3) only at speed of light.

Therefore, Planck mass is smaller than Fermi energy of cosmotomic electron.

$$m_{Planck} = 1.2209 \times 10^{28} eV$$

When seed of weaktron (bas mass of weaktron or seed mass of weaktron(cf.§6) is same as Planck mass) is accelerate by energy of active cosmotomic nucleus, this particle must be fly over light speed.

Therefore, we can find here that Einstein's special relativity is wrong.

The first order Fermi acceleration of active cosmotomic nucleus by maximum Lorentz factor of relativistic shock for a proton is

$$E_{\gamma ACN} = (7.51\times 10^{32} eV)(1.836 \times 10^{3})$$

$$= 1.38 \times 10^{36} eV \qquad 25\text{-}46$$

This energy is called Fermi energy of cosmotomic proton.

Sources of such cosmic rays (electron and related hadron) can be stars, supernova remnants and AGN.

However, here important point is that strong accelerators of cosmic rays by curve of force lines are supernova remnant, AGN and ACN.

Because present physics doesn't have calculable general relativity, it can be calculated only useless GZK limit by special relativity.

Therefore, cause of ultrahigh energy cosmic rays that are pre accelerated by curve of force lines cannot explain.

25.6. Solving the Cosmic Rays Knee Problem: What Is the Cause of the Cosmic Rays Knee?

By such calculation of CFLE Theory the 54 years old "cosmic rays knee problem" can be solved as below.

Roughly speaking, for every 10% increase in energy beyond 10^9 eV, the number of cosmic rays per unit area

falls by a factor of 1,000. However, if we look at the spectrum more closely we can see a *knee* at 3×10^{15} eV

(G. Khristiansen et al) and an *ankle* at 3×10^{18} eV (G.Khristiansen et al) as Figure 25-10-A.

Energy of supernovae electron is $E = 8.42 \times 10^{10} eV$ according to Eq.25-43.

This supernova electron could be accelerated by curved galactic field as much as $\gamma_{AGN} = g^5 C_c^5 \approx 10^5$ according to Eq.25-41.

After accelerating by galactic curvature factor energy of supernovae electron is increased

$$E = (8.42 \times 10^{10} eV)(9.13 \times 10^4) \rightarrow$$

$$E = \frac{7.69\times 10^{15} eV}{(1.5)^2} = 3.42 \times 10^{15} eV \qquad 25\text{-}47$$

Because of this increased energy is appeared cosmic rays knee.

When supernovae electron that created near cosmotomic nucleus is accelerated by cosmotomic curvature factor $\gamma_{ACN} = g^6 C_c^6 = (6.546)^6 (1.5)^6 \approx 10^6$, energy is increased

$$E = (8.42 \times 10^{10} eV)(8.65 \times 10^5) \rightarrow$$

$$E = (8.42 \times 10^{16})(92) = 7.28 \times 10^{18} eV$$

$$E = \frac{7.28\times 10^{18} eV}{(1.5)^2}) = 3.24 \times 10^{18} eV \qquad 25\text{-}48$$

where 92 is proton number of uranium.

This energy point is end point of galactic cosmic rays and start point of regular comotomic cosmic rays.

Observed knee value (G. Khristiansen et al) is

$$E_{knee} \approx 3 \times 10^{15} eV \qquad 25\text{-}49$$

Observed ankle value (G. Khristiansen et al) is

$$E_{ankle} \approx 3 \times 10^{18} eV \qquad 25\text{-}50$$

This good agreement means that CFLE theory is correct.

Therefore, essence of cosmic ray knee and ankle is curvature of each force lines as curvature of super gravitational field.

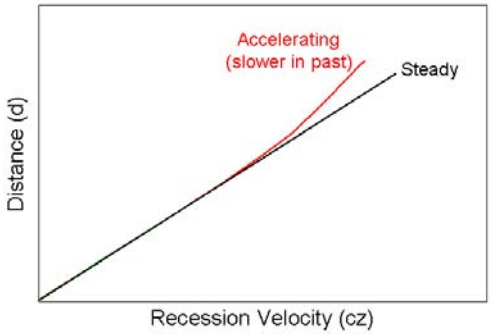

Accelerating Universe

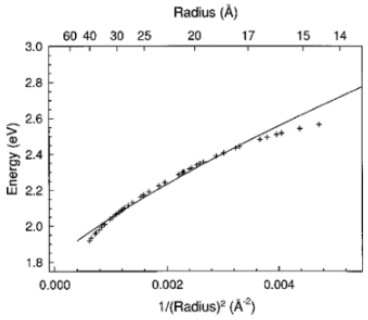

Energy of the first excited state ($1S_{3/2}1S_e$) in CDSe vs 1/radius^2.
The curve (solid line) obtained from theory is compared with PLE data (crosses). Physical review B Vol 52,No24,15 June 1996
D.J. Norris and M.G. Bawendi at Massachusetts Institute of Technology

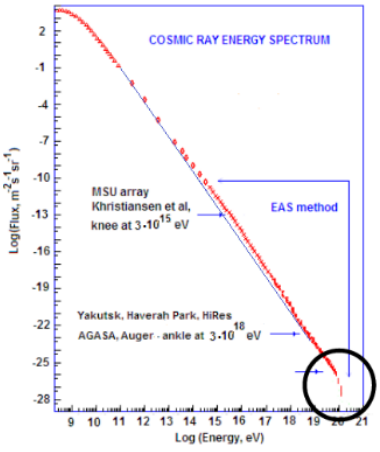

Similarity of three anomalies from different research fields

(from Figure 25-8 and Figure 25-10)

Finally, we can conclude that cause of mystery of first order Fermi acceleration and related cosmic ray knee problem is curvature of each force lines.

If Einstein and Einstein like physicists were, they would say only about problem of curvature of space-time continuum by super gravity or black hole instead curvature of each force lines.

Furthermore, they believe that when they can observe gravitational wave by detector of the Laser Interferometer Gravitational-Wave Observatory (LIGO) that is joint project between scientists at MIT, Caltech, and many other colleges and universities, Einstein's general relativity can be clearly confirmed. However, if they could observed gravitational wave as last evidence of general relativity by LIGO successfully, such fact cannot guarantee about existence of curve able space-time continuum as mentioned in §3(tests of deflection of light, Mercury's orbit, gravitational redshift, gravitational lensing, light travel time delay and frame-dragging).

Because principally detector of LIGO cannot distinguish between real motion of space-time continuum and real interaction of gravitational wave of bunch of real gravitational force line with all of observatory of LIGO, despite sensitivity of detector of LIGO is detectable relative change of one part in 10^{21} over a 100Hz bandwidth.

Therefore, it is expected that unmixable Einstein's general relativity with QED is demanded as before without meaningful results, when gravitational wave could be detected as motion of space-time continuum by detector of LIGO.

Because for $\mathrm{GZK\,limit}(\mathrm{E} = 5 \times 10^{19} eV)$ to calculate is used only Einstein's special relativity, GZK limit is useless and meaningless in the world of reference flame of curved force lines.

Furthermore, GZK limit obstruct right to infer.

If we could be free from such obstacle, by this successful quantitative explanation about cosmic rays paradox and cosmic rays knee problem with curvature of force lines, we can solve 108 years old mystery of the Tunguska event qualitatively and quantitatively.

25.7. Solving the Mystery of the Tunguska Event: What Is the Tunguska Cosmic Body?

The Tunguska event (TE) was a large explosion that occurred near the Podkamennaya Tunguska River (Central Siberia of the coordinates of the point usually called epicenter, 60° 53' 09" N, 101° 53' 40"E: Fast 1967), in what is now Krasnoyarsk Krai, Russia, on the morning 7:17 of 30 June 1908.

Figure 25-11

The explosion over the sparsely populated Eastern Siberian Taiga flattened 2,150±50 km^2 (~830 sq mi) of forest (Eighty millions trees were flattened, a great number of trees: 8×10^7 and bushes were burnt in a large part of the explosion area). Eyewitnesses described the flight of a "fire ball, bright as the sun". Seismic and pressure waves were recorded in many observatories throughout the world.

$$A_{Tunguska} = 2.150 \times 10^3 km^2 \pm 50 km^2 \qquad 25\text{-}51$$

Leonid.A. Kulik (1883~1942)

Damage from the 1908 Tunguska impact as documented by Leonid Kulik on his 1929 expedition to the epicenter.

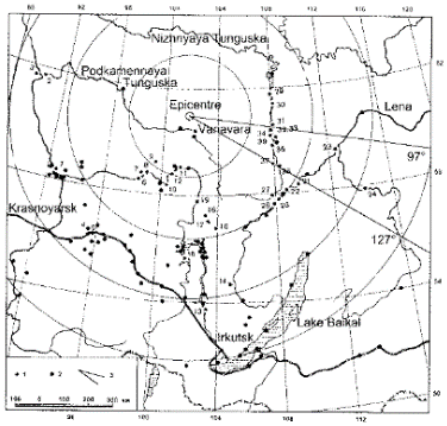

Map with the location of the more reliable witnesses of the Tunguska event: 1 – visual observations, 2 – acoustical records and barograms, 3 – azimuths spanning from 97° to 127°, used in the present calculations.

Figure 25-12

However, the most interesting thing is that they have not found a crater left by a meteorite impact on Earth. Another oddity of the Tunguska event was that the forest was knocked over a large area close to the presumed site of a meteorite (The energy release, equivalent to 10-15 Mt of TNT that corresponds to about few thousand times the Hiroshima bomb energy: height of the explosion 5-10km, though the values for the last two parameters are estimated with great uncertainty)), but at the very epicenter of the explosion it remained standing trees as Figure 25-12.

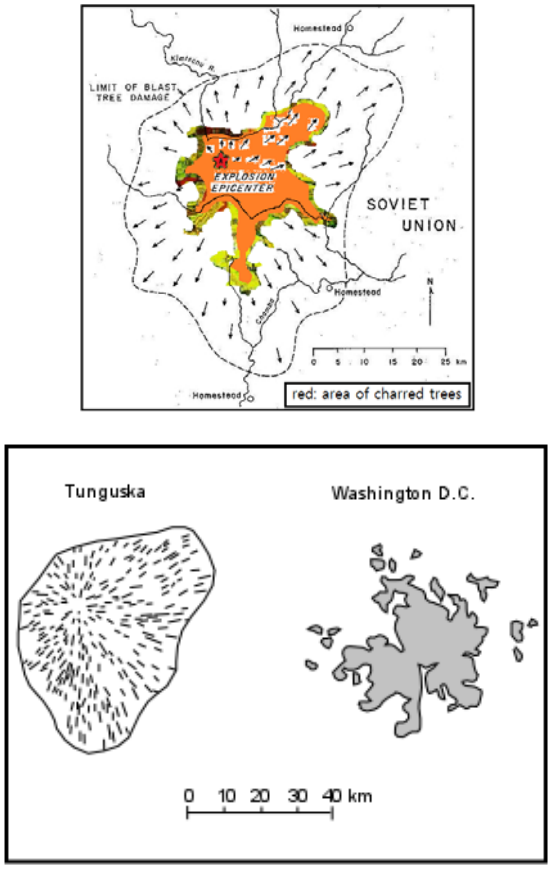

Washington D.C area compared with that the Tunguska devastation

Figure 25-13

Furthermore, on the night of 30 June 1908 and the next three nights, aurora-like displays were seen in northern Europe. W. F. Denning wrote, "certain features of the glows struck me as essentially different from exhibitions of normal Auroræ Boreales."

Such bright nights were observed over much of Eurasia. These different phenomena, initially considered non-correlated, were subsequently linked together as different aspects of the “Tunguska event”

Almost one century has elapsed and scientists are still searching for a commonly accepted explanation of this event. Several reviews and books summarize the results acquired by the intensive investigations of the last century, e.g. Kulik (1922, 1939, 1940), Landsberg (1924), Krinov (1949, 1966), Gallant (1995), Trayner (1997), Riccobono

(2000), Bronshten (2000), Vasilyev (1998, 2004) and Verma (2005). Despite great efforts, the TE remains a conundrum.

The most plausible explanation of the event considers the explosion in the atmosphere of a "Tunguska Cosmic Body" (TCB), probably a comet (cometary air burst) or an asteroid-like meteorite.

Seismic records from Irkutsk, Tashkent, and Tiflis were published together, two years after the event (Levitskij 1910), those from Jena, three years later. The first paper that connected to the TE the origin of these seismic waves was published only in 1925 (Voznesenskij 1925). Similarly, the barograms recorded in 1908 in a great number of observatories throughout the world, were associated with the TE some twenty years later (Whipple 1930; Astapovich 1933).

However, neither macroscopic fragments of the cosmic body, nor a typical signature of an impact, like a crater as Figure 25-14, have ever been found in an area of 15 000km^2, so that the nature and composition of the TCB and the dynamic of the event have not yet been clarified.

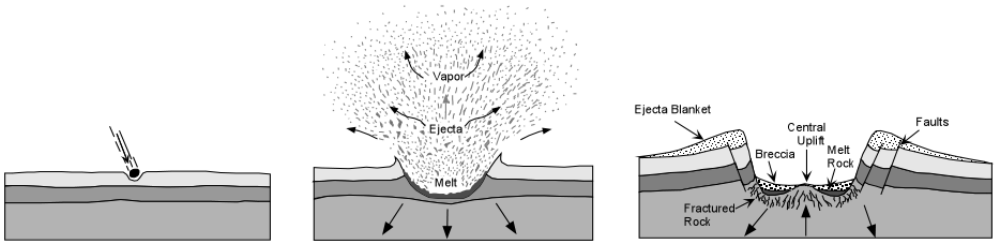

Figure 25-14

Figure 25-15 shows one crate that is called The Barringer Meteorite Crater of Arizona, USA.

This crater was formed by the impact of an iron-nickel meteorite impacting into the high arid plains of the Colorado Plateau about 50,000 years ago. The body, estimated to have been about 50 meters in diameter and weighed several hundred thousand metric tons, was traveling on the order of 15 kilometers per second and impacted with a kinetic energy of some 30-40 megatons of TNT equivalent. The result of the collision was to form, in just a second or so, a large bowl-shaped crater 1.2 kilometers across and over 150 meters deep.

Figure 25-15

Nearly 100 million tons of rock were thrown out to form a continuous ejecta blanket around the crater. Strong air and ground shock waves were felt for tens of kilometers away. Relatively little erosion has occurred leaving the crater well-preserved. The Barringer Meteorite Crater now serves as the prototype of the classic bowl-shaped impact crater found thruout in our solar system. It has played a dominant role in public education, NASA planetary studies, and scientific research in impact cratering.

However, today's epicenter of Tunguska event is flat as

The pastoral picture above (taken by L. Pelekhan) depicts a peaceful meadow in Siberia. However, 108 years ago, on June 30, 1908, this exact spot was the epicenter of a large explosion from some type of celestial body–a meteor, asteroid or fragment of a comet–which struck the Earth. This incident has come to be known as the "Tunguska event," named after the place where it occurred.

Figure 25-16

Such contradiction to avoid, air burst of stony asteroid, meteorite and comet was suggested as Figure 25-17.

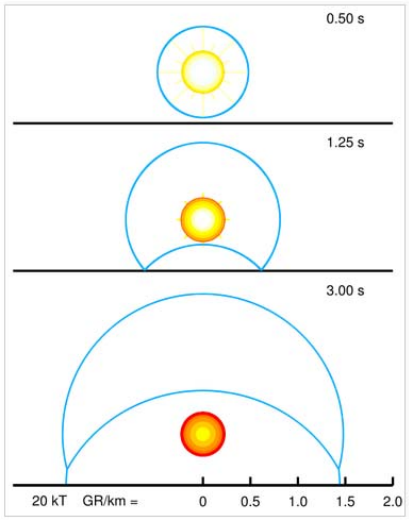

Figure 25-17

However, the air burst is usually several hundred to a few thousand feet (100 to 1,000 m) above the hypocenter to allow the shockwave of the fission or fusion driven explosion to bounce off the ground and back into itself, creating a shockwave that is more forceful than one from a detonation at ground level("mach stem" only occurs near ground level, and is similar in shape to the letter Y when viewed from the side). Here, most important point is that The height of the Tunguska explosion is closely related to the value of the energy emitted, usually estimated to be equal to about 10–15 MT (Hunt 1960; Ben-Menahem 1975), although some authors consider the energy value to be higher, up to 30-50Mt (Pasechnik 1971, 1976, 1986). In agreement with the first energy range, which seems to have more solid grounds, the height of the Tunguska explosion was found equal to 6–14 km. Furthermore, any related abnormal material of micro scale was not observed in green land ice core after 1908.

Therefore, to avoid such contradiction, recently, some “alternative” approaches were presented to explain the TE.

The first is a tectonic interpretation (e.g. Ol’khovatov 2002), which considers the coupling between tectonic and atmospheric processes in a “very rare combination of favorable geophysical factors.

Another recent work that should be mentioned is the “kimberlite interpretation” (Kundt 2001), which considers the TE as caused by the tectonic outburst of some 10 megaton of natural gas.

The main idea of this latter work is contradicted by at least two facts. The first and more obvious point against the hypothesis of an explosion from the ground is that the eyewitness testimonies describe the trajectory of a bolide crossing the sky.

Further approaches among 160 hypotheses are collision with a miniature black hole or piece of antimatter even UFO Explosion.

However, CFLE theory can solve simply this 108 years old Tunguska mystery.

The answer is air shower by super ultrahigh energy cosmic ray.

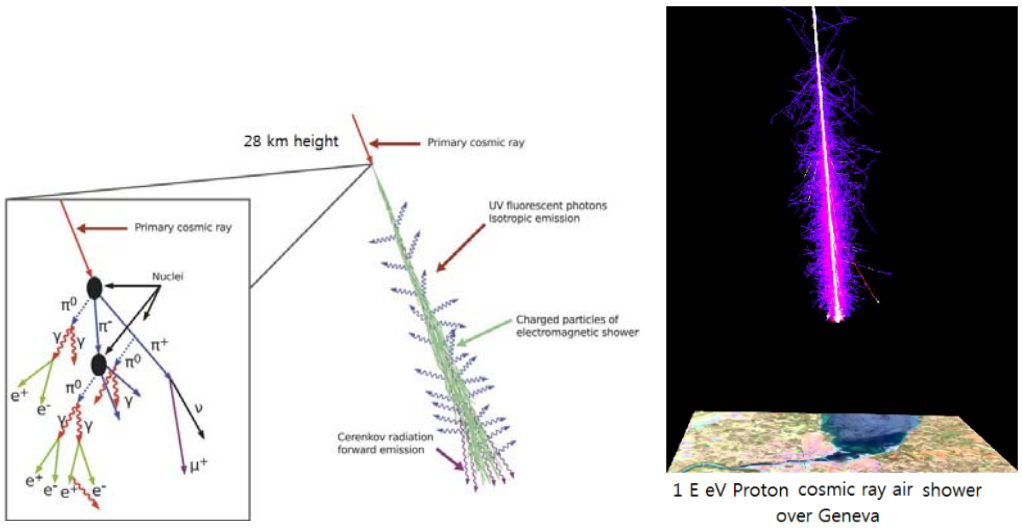

Figure 25-18

An air shower is an extensive (many kilometers wide) cascade of ionized particles and electromagnetic radiation produced in the atmosphere when a *primary* cosmic ray (i.e. one of extraterrestrial origin) enters the atmosphere. The term *cascade* means that the incident particle, which could be a proton, a nucleus, an electron, a photon, or (rarely) a positron, strikes an atom's nucleus in the air so as to produce

many energetic hadrons. The unstable hadrons decay in the air speedily into other particles and electromagnetic radiation, which are part of the shower components. The secondary radiation rains down, including x-rays, muons, protons, antiprotons, alpha particles, pions, electrons, positrons, and neutrons as Figure 25-18-A (cf. Section S25.7).

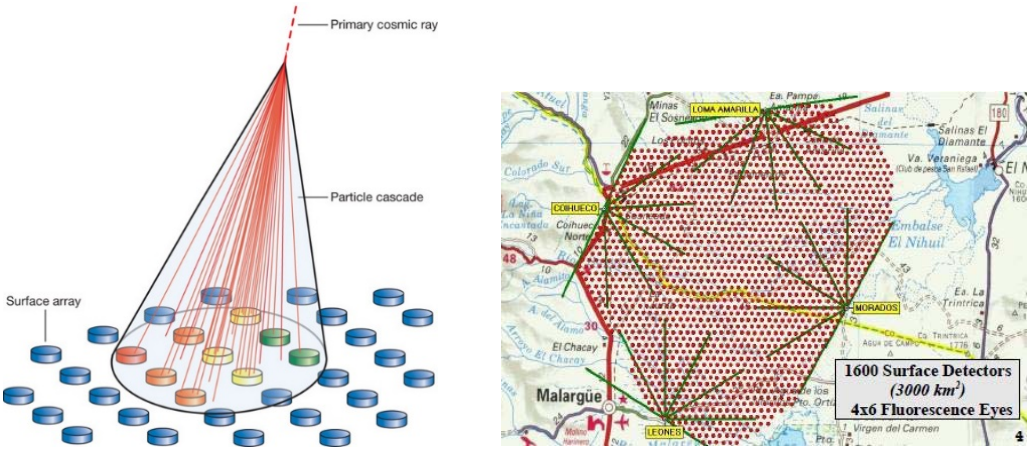

A B

Figure 25-19

The original particle arrives with high energy and hence a velocity near the speed of light, so the products of the collisions tend also to move generally in the same direction as the primary, while to some extent spreading sidewise. In addition, the secondary particles produce a widespread flash of light in forward direction due to the Cherenkov effect, as well as fluorescence light that is emitted isotropically from the excitation of nitrogen molecules. The particle cascade and the light produced in the atmosphere can be detected with surface detector arrays and optical telescopes. Surface detectors typically use Cherenkov detectors or Scintillation counters to detect the charged secondary particles at ground level as Figure 25-19-A.Figure 25-19-B is the Pierre Auger Observatory that's area is larger than Tunguska explosion's area!!!

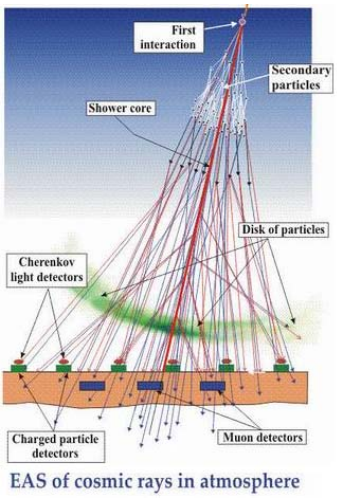

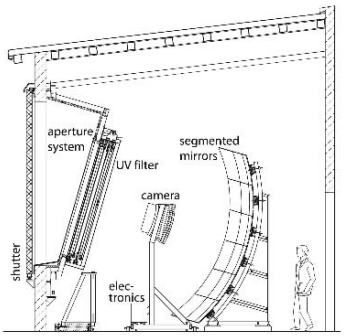

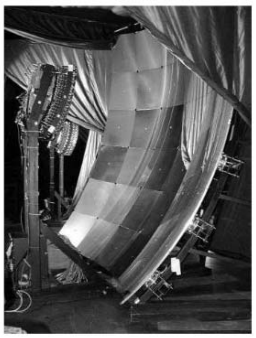

Schematic setup and picture of a fluoresence camera in an FD building
(by Marius Grigat from Wald bröl 10, 06,2011)

A B

Figure 25-20

Figure 25-20-A shows distribution of detectors. Figure 25-20-B show a fluorescence camera in an Fluorescence Detector Building.

A

B

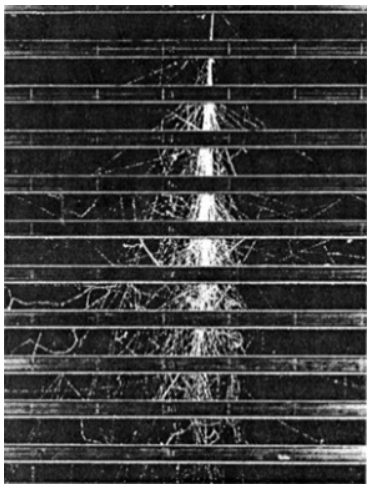

C

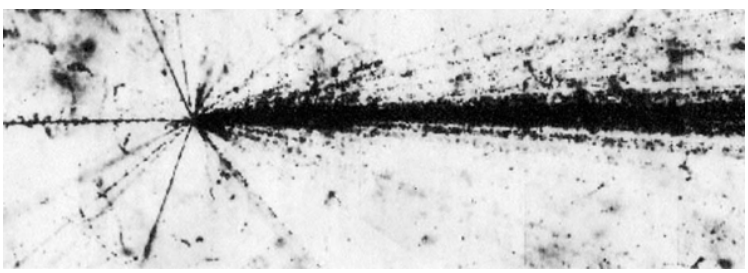

Figure 25-21

Historically speaking, in a balloon at an altitude of 5000 meters, Victor F. Hess (1833-1964) in Figure 25-21-A, the father of cosmic-ray research, discovered "penetrating radiation" coming from space. His research was the first of many adventurous journeys made by physicists to study cosmic rays.
Figure25-21-B show a cloud chamber photograph (MIT cosmic ray group) of a particle traversing a series of brass plates demonstrates that a single particle can indeed give rise to multiple secondary particles.
Figure 25-21-C show a collision between a high energy cosmic ray particle and an atom in a photographic emulsion as viewed through a microscope.

Now, all of mysterious anomalies of Tunguska event can be explained by model of super ultrahigh energy cosmic ray air shower of CFLE theory qualitatively and quantitatively.

In 1908, the attention of astronomers and geophysicists in Europe and Asia was drawn to some unusual phenomena, such as 3bright nights, noctilucent clouds, brilliant colorful sunsets and other observations. It is difficult to conclude that some of these phenomena are really "anomalous". This is confirmed by the global character of this phenomenon and by polarization measurements. The "global" character of the phenomenon, observed in the nights beginning on 30 June and 1 July 1908 are illustrated in Fig. 25-22-Aand 25-23-A (Vasilyev and Fast 1976, from the paper of G. Longo).

Stations where anomalous bright nights were observed the 30 June/1 July 1908

A

Aurora night of June 22,2015 in Canada by Marie Carmen

B

Figure 25-22

As can be seen, the 3 bright nights were observed on an area of about 12 million km^2, from the longitude 6.5° W (Armagh, Ireland; see Fig. 25-22-A) up to 92.9° E (Krasnoyarsk) and from the latitude 41° N (Tashkent) up to 60° N (Petersburg).

Photos of Figure 25-23-A show real character of 3 bright nights by Tunguska event.

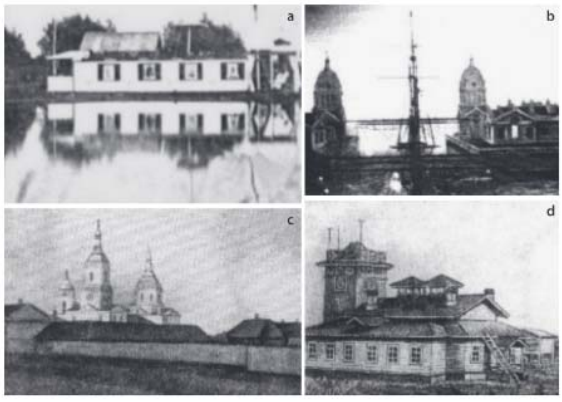

Photos taken during the bright night of 30 June 1908 in (**a**) Armagh, (**b**) Greenwich, and (**c**) Tambow. **d** The Irkutsk observatory

A

Isotropic Emission of UV Fluorescence Photons

B

Figure 25-23

If the 3 bright nights are due to dust in the atmosphere, the light reflected should be polarized. Busch (1908a, b) measured the daylight polarization in Arnsberg (Germany). His results indicate an absence of the effect in the first half of 1908 up to 28 June, a strong effect the 1 July that gradually disappears up to 25 July. The conclusions of Igor. Zotkin were that it is difficult to accept that dust particles could reach Great Britain from Tunguska in 22 hours. There was a sharp exponential decrease in the intensity of the atmospheric anomalies after the first of July 1908. This suggests that the major cause of the anomalies was due to photo chemical reactions.

However, model of cosmic ray air shower of CFLE theory can explain about 3bright nights and fire ball as Eyewitnesses described the flight of a “cylinder formic fire ball, bright as the sun” same times.

Cause of light of “cylinder formic fireball, bright as the sun” is super luminous forward Cherenkov radiation from air shower as Figure 25-18-B.

This is satisfactorily explanation about phenomenon of fire ball of Tunguska event.

Cause of 3 bright nights is UV fluorescent photons isotropic emission from ultra-huger air shower than Figure 25-23-B.

Fluorescence is the emission of light by a substance that has absorbed light or other electromagnetic radiation. It is a form of luminescence. In most cases, the emitted light has a longer wavelength, and therefore lower energy, than the absorbed radiation. The most striking example of fluorescence occurs when the absorbed radiation is in the ultraviolet region of the spectrum, and thus invisible to the human eye, while the emitted light is in the visible region, which gives the fluorescent substance a distinct color that can only be seen when exposed to UV light. Furthermore, unlike phosphorescence, where the substance would continue to glow and emit light for some time after the radiation source has been turned off, fluorescent materials would cease to glow immediately upon removal of the excitation source.

Now, we can accept how effect of 3 bright nights that at midnight, it was possible to read the newspaper without artificial Lights were described in many papers (e.g., De Roy 1908; Shenrock 1908; Süring 1908; Svyatskij 1908), could reach Great Britain from Tunguska in 22 hours and why absence of the effect of bright night appeared in the first half of 1908 up to 28 June, a strong effect the 1 July that gradually disappears up to 25 July.

Simply to say, cause of bright night is not dust from asteroid, meteorite or comet, but fluorescence of air by UV light from cosmic ray air shower, so to speak kind of aurora as Figure 25-22-B

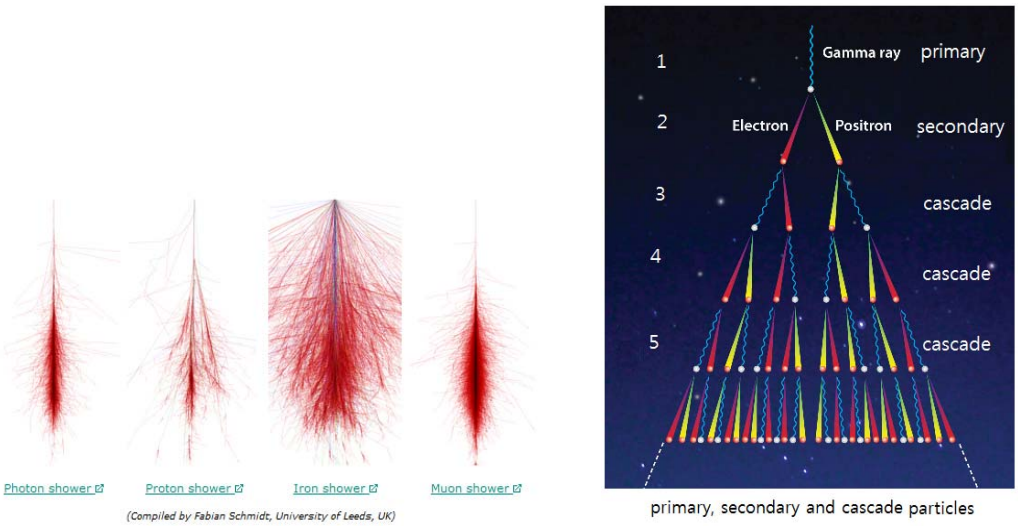

A **B**

Figure 25-24

Figure 25-24-A show different air shower type by photon, proton, iron and muon.

Figure 25-24-B show what is called primary, secondary and cascade particles of CFLE theory.

Figure 25-25 show air shower simulation by Marco Alania, Ignacio J. Araya, Adolfo V. Chamorro Gomez, Humberto Martinez Huerta, Alejandra Parra Flores and Johannes Knapp at Universidad Nacional de Ingenie peru, Pontificia Universidad Catolica de Chile, Universidad Autonoma de Puebla Mexico,University of Leeds, United Kingdom with the CORSIKA EAS simulation Program.

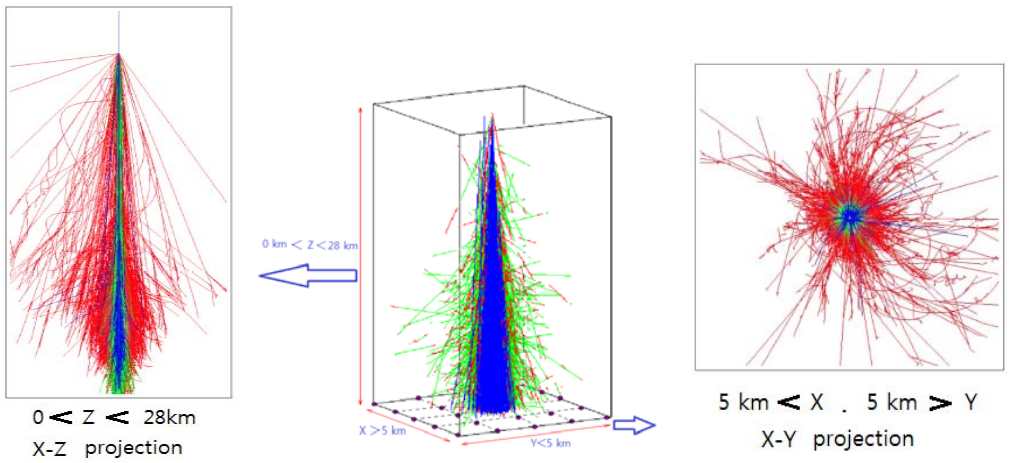

Iron-induced air shower at $\mathbf{E = 1 \times 10^{13} eV}$, $\mathbf{\theta = 0^0}$

Figure 25-25

Therefore, this simulation is called **the CORSIKA air shower simulation.**

When air shower by proton (Figure 25-26 -A) occur in magnetic field (Figure 25-26-B), positive charged particle should be fly to north and negative charged particle should be south.

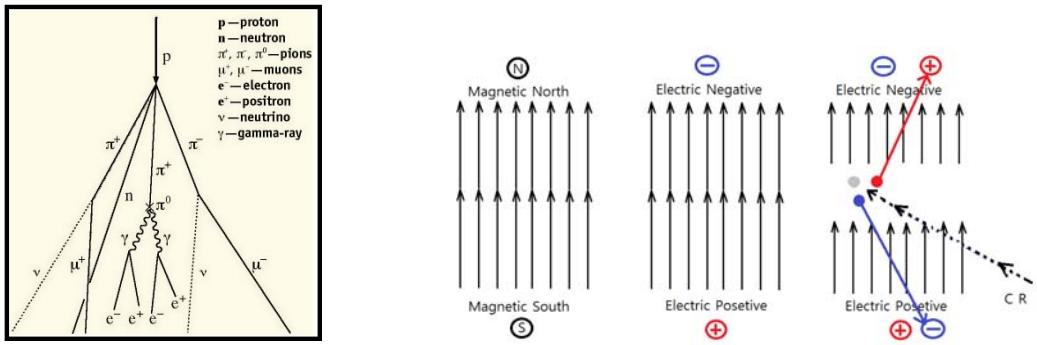

Figure 25-26

Therefore, if Tunguska explosion were occurred by cosmic ray air shower by super ultrahigh energy proton as Figure 25-26-A, we can expect four explosion direction by four components secondary particles as Figure 25-27.

Trace by $\pm$ charged pion ($\boldsymbol{\pi^{\pm}: m = 139.57\ MeV}$) of secondary particles should be shorter than secondary neutral particles (neutron $\mathbf{n}$ and neutral pion $\boldsymbol{\pi^0}$) because of their charge. Trace of secondary particle of neutral pion ($\boldsymbol{\pi^0: m} = 134.98\ \boldsymbol{MeV}$)is shorter than secondary particle of neutron($\mathbf{n: m = 939.57 MeV}$) because of their mass difference.

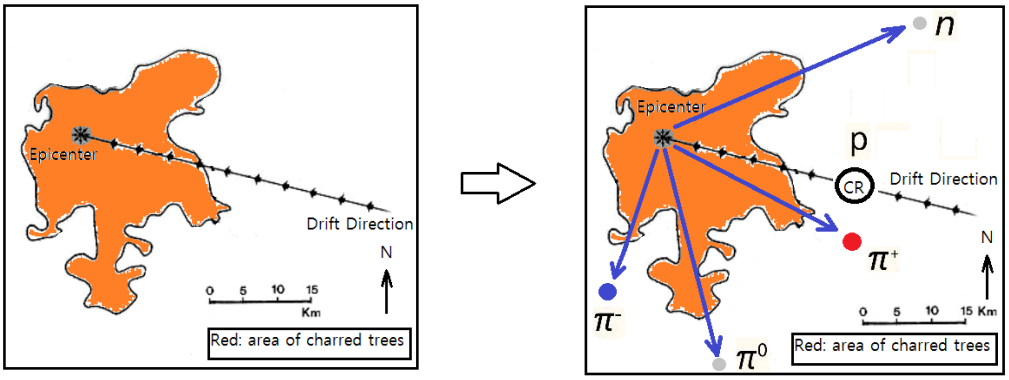

A Only Charred Area B

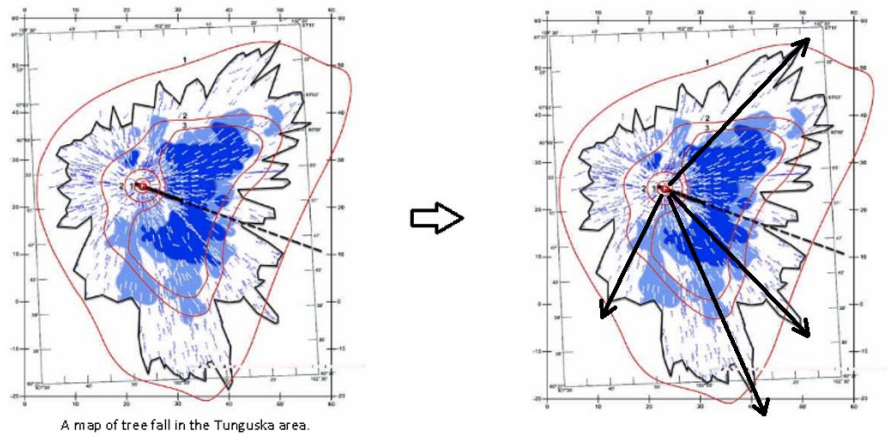

C Total Damage Area D

Figure 25-27

Now, we can understand why two flat main epicenter appeared in Tunguska explosion site as L.A. Kulik suggested as Figure 25-28-B.

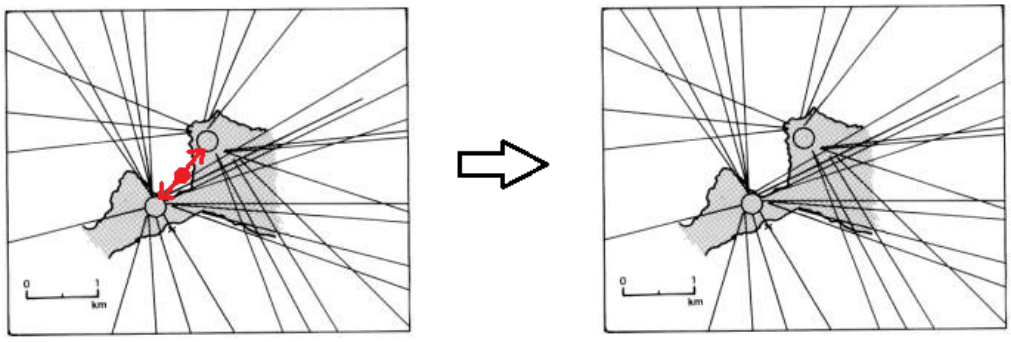

A B

Figure 25-28-B is based on examination of the results of the aerial photographic survey of the central part of the Tunguska region, carried out in 1938 under the direction of Kulik. The survey consisted in 1,500 good quality photographs, on a scale 1:4700, covering an area of 250 km2 of devastated forest (Kulik 1939, Kulik 1940). As stated by Krinov (1966), "the individual flattened trees were clearly seen in the photographs. Even in the unenlarged prints, the directions in which their tops and roots were facing could be easily made out". These directions, clearly showing the general radial pattern of the tree fall, made it possible, according to Kulik, to identify from 2 to 4 secondary centers of wave propagation. The two main secondary centers, located in the western part of the Southern swamp, are shown in Fig 25-28-B, where the straight lines indicate the directions of the fallen trees. Figure 25-28-B is drawn on the basis of Kulik's Figure (1939) with the addition of some lines taken from the subsequent papers (Kulik 1940, Krinov 1949), where the directions of overthrown trees were indicated with the aid of threads extended over a field mosaic photographic chart of the region.

Figure 25-28

Figure 25-28-B show the two flat main secondary epicenters of explosive propagation (circles) according to L.A. Kulik (1939, 1940, Kulik's interpretation of the felled forest area on the basis of a large-scale photographic air survey of 1938: L.A. Kulik, 1939, not only corroborated the complex vector structure of the epicenter area, but also suggested at least two or four sub epicenters). The straight lines indicate the direction of the fallen trees. The shaded region correspond to the western part of the Southern swamp. The cross shows the position of the trees$n^0 5\ and\ n^0 6$.

Figure 25-28-A show a particle before impact on Earth surface (red dot). Before impact on Earth surface pair particles created by collision between cosmic ray particle and atom of Earth atmosphere.

After pair creation of particles impact on Earth surface.

Therefore, there can be occurred two flat main epicenter and other accessory epicenter by impact of third cascade particles.

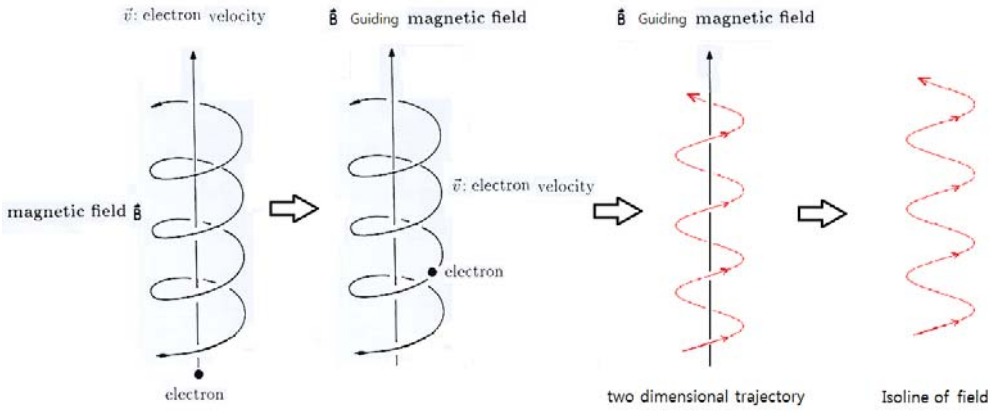

Typical moving trajectory of charged particle along guide magnetic field.

Figure 25-29

Figure 25-29 show typical moving trajectory of charged particle in Earth's magnetic field as guide magnetic field by Charged particle.

With this mechanism of classical electrodynanics we can explain mystery of Isolines of the Tunguska tree fall pattern.

Figure 25-30 shows that Isolines of the field of the azimuths of felled trees of Tunguska ,in degrees to the east of the magnetic North(The azimuth 0^0 corresponds to the direction of the magnetic North). The values printed diagonally are the azimuths calculated for 1 km^2 surfaces by the interpolating the measured average azimuth-values.

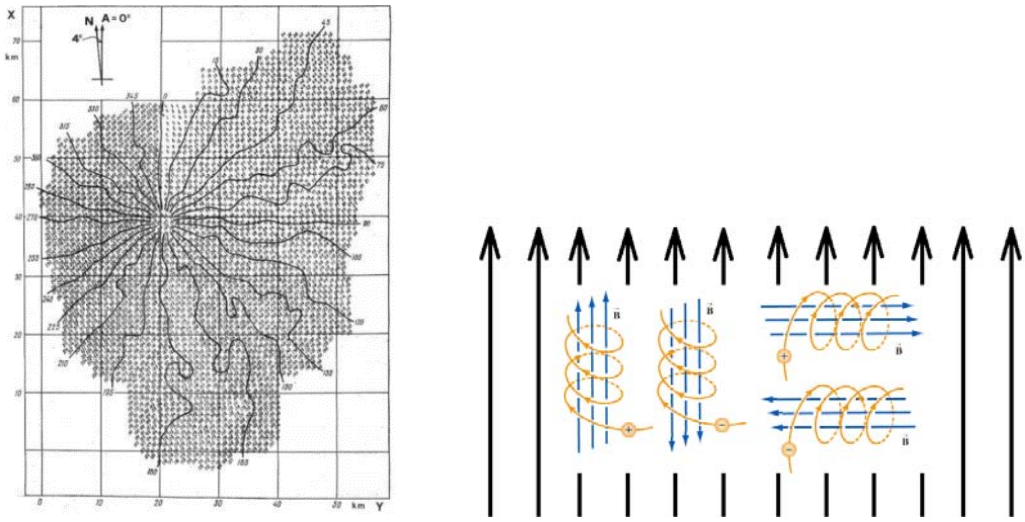

A B

Isolines of the Tunguska tree fall pattern, taken from Serra et al (1994): Connected are points on the map in whose $1km^2$ neighborhoods the felled trees had the same average orientation, as note on outer edge of the destruction area (in degree). Obvious is a coarsely radial pattern with strong local deviations.

Figure 25-30

Figure 25-30-B show how local magnetic anomaly (local magnetic reversal) can be occurred in Tunguska explosion area.

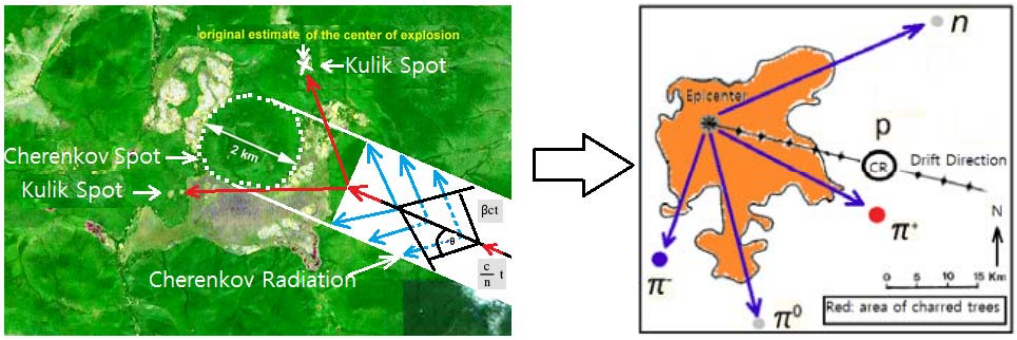

A B

Figure 25-31

Figure 25-31-A show trajectories of other cascade particles groups in X-Y plain of the CORSIKA air shower simulation.

According to this simulation and property of other cascade particles from air shower as muons ($\mu^{\pm}: m = 105.66\, MeV$) and neutrinos ($\nu^{\pm}: m_e = 0.043$ eV, $m_\mu = 0.163$ eV, $m_\tau = 0.331$eV (cf. §7.7)) we can understand why standing trees remained near the epicenter(see Figure 25-12: photo by L.A.Kulik 1929) despite strong energy of 10-50 Mt (2600 time stronger than Hiroshima atom bomb) released at that time.

Such anomaly can be explained because muon and neutrino can penetrate without strong interaction with usual material of standing trees similarly as Hiroshima nuclear explosion. During eighty millions trees were flattened by charged and massive particles from air shower, remain standing trees were only penetrated by light leptonic particles that cannot strong interact with standing trees.

A Pothograph (from 26 July 1999) from the point usually called "epicenter" of the 1908 Tunguska explosion

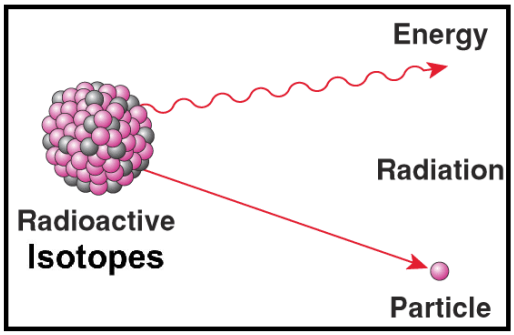

B usual atom is changed radioactive Isotope by secondary particles from ultra high energy cosmic ray air shower

Figure 25-32

Figure 25-32-A (from “Exploring the site of the Tunguska impact” by G. Longo, E. Bonatti, M.D. Martino, L. Foschini and L. Gasperini) show two flat main epicenter of Tunguska event.

Now, we can understand why such two flat epicenter was remained instead meteorite type crater, despite eighty millions trees were flattened.

Because impact material is not meteorite and asteroid but Cherenkov photon and micro size cascade particles from air shower (cf. Section S25.7).

Therefore, in CFLE theory such flat epicenters are called Cherenkov-kulik spots (CKS).

However, we have to conclude that "explosion by Cherenkov photon and secondary particles” from the cosmic ray air shower (CRAS) with flat epicenter initiated a seismic wave that was recorded in the cities of Irkutsk, Tashkent, Tbilisi and Jena. There also were pressure disturbances (Astapovich, I.S., 1933; Whipple, F.W., 1934) 5.9(0.9 minutes (or, according to another estimate, 6.6 (0.2 min.) after the explosion. It is not unthinkable scenario.

One another of the most striking geophysical anomaly associated with the Tunguska explosion is the local geomagnetic disturbance detected shortly after the explosion in Irkutsk, although not recorded by any other geophysical observatory in the world existing at that time (Plekhanov, G.F. et al., 1960; 1961; Ivanov, K.G., 1961; 1961 a; 1962; 1964; Obashev, S.O., 1961; Zhuravlev, V.K., 1963; Kovalevsky, A.F., 1963).

A local magnetic storm was registered and persisted for more than four hours and caused geomagnetic disturbances in the atmosphere similar to those that follow nuclear explosions (Pasechnik, I.P., 1976; Ivanov, K.G., 1961). Now, we can understand why geomagnetic disturbances in the atmosphere occurred as nuclear explosions, because explosion by CRAS charged and radioactive particles was emitted as nuclear explosions.

Now, we can expect that by this emitted energetic secondary and charged cascade particles from air shower can be created radioactive isotopes as Figure 25-32-B.

Such radioactive isotope is called Tunguska type radioactive isotopes or Tunguska type radionuclide.

A radionuclide (radioactive nuclide, radioisotope or radioactive isotope) is an atom that has excess nuclear energy, making it unstable. This excess energy can either create and emit, from the nucleus, new radiation (gamma radiation) or a new particle (alpha particle or beta particle), or transfer this excess energy to one of its electrons, causing it to be ejected (conversion electron). During this process, the radionuclide is said to undergo radioactive decay. These emissions constitute ionizing radiation. The unstable nucleus is more stable following the emission, but sometimes will undergo further decay. Radioactive decay is a random process at the level of single atoms: it is impossible to predict when one particular atom will decay. However, for a collection of atoms of a single element the decay rate, and thus the half-life (t1/2) for that collection can be calculated from their measured decay constants. The duration of the half-lives of radioactive atoms have no known limits; the time range is over 55 orders of magnitude. Radionuclides both occur naturally and are artificially made using nuclear reactors, cyclotrons, particle accelerators or radionuclide generators. There are about 650 radionuclides with half-lives longer than 60 minutes. Of these, 34 are primordial radionuclides that existed before the creation of the solar system, and there are another 50 radionuclides detectable in nature as daughters of these, or produced naturally on Earth by cosmic radiation. More than 2400 radionuclides have half-lives less than 60 minutes. All chemical elements have radionuclides. Even the lightest element, hydrogen, has a well-known radionuclide, tritium. Elements heavier than lead, and the elements technetium and promethium, exist only as radionuclides. Radionuclides can have both beneficial and harmful effects on living organisms. Radioactive isotope or radioisotope, natural or artificially created isotope of a chemical element having an unstable nucleus that decays, emitting alpha, beta, or gamma rays until stability is reached. The stable end product is a nonradioactive isotope of another element, i.e., radium-226 decays finally to lead-206.

With this radionuclide that was created by cosmic ray air shower, we can explain genetic anomalies and vegetation anomaly of Tunguska event

One of great mysteries of the Tunguska event was its genetic impact. Some genetic anomalies were reported (Z.K. Silagadze in the "Tunguska genetic anomaly and electrophonic meteors" arXive:astro-ph/0311337v2.16.Nov.2003) in the plants, insects and people of the Tunguska region. Remarkably, the increased rate of biological mutations was found not only within the epicenter area, but also along the trajectory of the Tunguska Space Body (TSB). At that no traces of radioactivity were found, which could be reliably associated with the Tunguska event.

Therefore, the main hypotheses about the nature of the TCB, a stony asteroid, a comet nucleus or a carbonaceous chondrite, readily explain the absence of radioactivity but give no clues how to deal with the genetic anomaly. A choice between these hypotheses, as far as the genetic anomaly was concerned, was like to the choice between ``blue devil, green devil and speckled devil'', to quote late Academician N.V. Vasilyev. Therefore, for the origin of the Tunguska genetic anomaly to explain was assumed even electrophonic meteors.

Of course, now, we don't need such meteors because iridium and other related material from such cosmic bodies cannot be observed in Greenland Ice core after the 1908.

There were two main types of genetic impacts observed. The first type includes accelerated growth of young and survived trees on a vast territory, as well as quick revival of the taiga after the explosion.

The second type of effects is related to the usual genetic impact of the Tunguska explosion. Already participants of Kulik's first expeditions made some observations about forest recovery in the catastrophe area. In various years the impressions were different (Vasilyev 1999): in 1929-1930 the taiga seemed depressed in this area, while in 1953 no signs of growth deceleration were seen in comparison with neighboring regions. The first systematic pilot study of growth of the tree vegetation in the catastrophe region was performed during 1958 expedition (Vasilyev 1999). Anomalously large tree ring widths up to 9 mm were found in young specimens which were germinated after the catastrophe, while the average width of the growth rings before the catastrophe was only 0.2-1.0 mm. Besides the young trees, the accelerated growth was observed also for the survived old trees.

Leonid. A. Kulik
(1883-1942)

Pavel Cherenkov
(1904-1990)

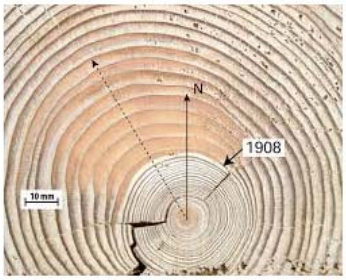

Tree rings were analysed in wood sample collected from some of the few surviving trees found close to the epicenter within 4-5 km of the Tunguska event that occured on the 30 june 1908

A B

Figure 25-33

Tree-ring growth of Figure 25-33-B (from "The origin of Lake Cheko and the 1908 Tunguska event recorded by forest trees" by Luca Gasperini, Carlo Stanghellini and Romano Serra) shows a depression starting in the year after the event and continuing during a 5-6 year period. The cause of the anomalous growth remained controversial.
However, CFLE theory can explain anomaly of accelerated growth of young trees. Energy source for accelerated growth of young trees is emission light including alpha, beta, or gamma rays from unstable nucleus of radioactive isotope decay that was created by high energetic secondary particles and cascade particles from cosmic ray air shower as Figure 25-32-B until stability is reached.
Therefore, half-life time $t_{1/2}$ of radioactive isotope for accelerated growth of trees should be $t_{1/2} = 5 - 6$ years
as Figure 25-33-B(0.2mm tree ring widths was enlarged 9mm 5-6 years long and next 5-6 years widths was changed half value of 9 mm…etc.) decay energy of radioactive isotope should be used for biochemical reaction for accelerated vegetation as $N_2 \rightarrow N + O \rightarrow NO_3$too.

Genetic consequences of the Tunguska event was the most controversial subject. In sixties some experiments were performed in Novosibirsk to find genetic effects of ionizing radiation on pines. Among various changes, the most prominent effect was an increased occurrence of 3-needle cluster pines, while usually the pine used in experiments had 2-needle clusters.

Cause of such mutation by damage of DNA sequence is decay of unstable radioactive isotope that was created by super ultrahigh energetic cosmic ray air shower.

Reported genetic anomaly in the people of the Tunguska region (native Evenki and Russian) must be results of radiation injury as Hiroshima radiation injury after nuclear explosion by unstable radioactive isotope that was created by super ultrahigh energetic cosmic ray air shower.

Now, we can surely suppose that lot of the people around Tunguska explosion was troubled by acute radiation syndrome just after super explosion.

Acute radiation syndrome (ARS), also known as radiation poisoning, radiation sickness or radiation toxicity, is a collection of health effects which present within 24 hours of exposure to high amounts of ionizing radiation. The radiation causes cellular degradation due to damage to DNA and other key molecular structures within the cells in various tissues; this destruction, particularly as it affects ability of cells to divide normally, in turn causes the symptoms. The symptoms can begin within one or two hours and may last for several months. The terms refer to acute medical problems rather than ones that develop after a prolonged period.

The onset and type of symptoms depends on the radiation exposure. Relatively smaller doses result in gastrointestinal effects, such as nausea and vomiting, and symptoms related to falling blood counts, and predisposition to infection and bleeding. Relatively larger doses can result in neurological effects and rapid death. Treatment of acute radiation syndrome is generally supportive with blood transfusions and antibiotics, with some more aggressive treatments, such as bone marrow transfusions, being required in extreme cases.

More important point is that similar symptoms may appear months to years after exposure as chronic radiation syndrome when the dose rate is too low to cause the acute form. Radiation exposure can also increase the probability of developing some other diseases, mainly different types of cancers. These diseases are sometimes referred to as radiation sickness, but they are never included in the term acute radiation syndrome.

Therefore, we can suppose that related different kind of isotope anomalies should be found there.

That is "Isotope anomalies of carbon, hydrogen and nitrogen in peat from the area of the Tunguska cosmic body explosion 1908" was reported by kolesnikov EM, B ö ttger T, Hiller A. Junge FW and kolesnikova NV at a Geological Faculty of Moscow state university in 1996 Dec.

Their report give us consistent conviction about cause of Tunguska explosion.

Here, important point is that "abstract peat profiles from the area of the Tunguska explosion epicenter indicate significant carbon and hydrogen isotope effects which are clearly associated with the zone of the 1908 catastrophe and which cannot be attributed to any known terrestrial processes."

The assumption of electrophonic meteor was denied by "Discovery of Iridium and other element Anomalies by the 1908 Tunguska Explosion" by Hou Quanlin and Ma Peixue at the Institute of High energy Physics, Chinese Academy of science and by "No iridium anomaly after the 1908 Tunguska impact: Evidence from a Greenland ice core" by Kaare .L. Rasmussen, Henrk .B .Clausen and Gregory. W. Kallemeyn in 15.Jun. 2012.

If iridium anomaly were found too Greenland ice core after the 1908, this assumption of electro phonic meteor should be truth.

However, Kaare .L. Rasmussen, Henrk .B .Clausen and Gregory. W. Kallemeyn they cannot find Iridium anomaly after the 1908 Tunguska explosion in Green land ice core

This means that cause of this anomaly must be only local anomaly of Tunguska explosion area.

Therefore, we have to be supposed that iridium anomaly of Tunguska region occur by local bombardment of secondary and cascade particles from super ultrahigh cosmic ray air shower or result of ancient volcano eruption.

Identity of Tunguska Cosmic Body (TCB) is only one energetic proton as primary cosmic ray by CFLE theory.

So far all of Tunguska anomalies is explained by results of impact of energetic particles from cosmic ray air shower only qualitatively.

However, CFLE theory can predict and calculate quantitatively how big blast energy of cosmic ray of Tunguska explosion is as below.

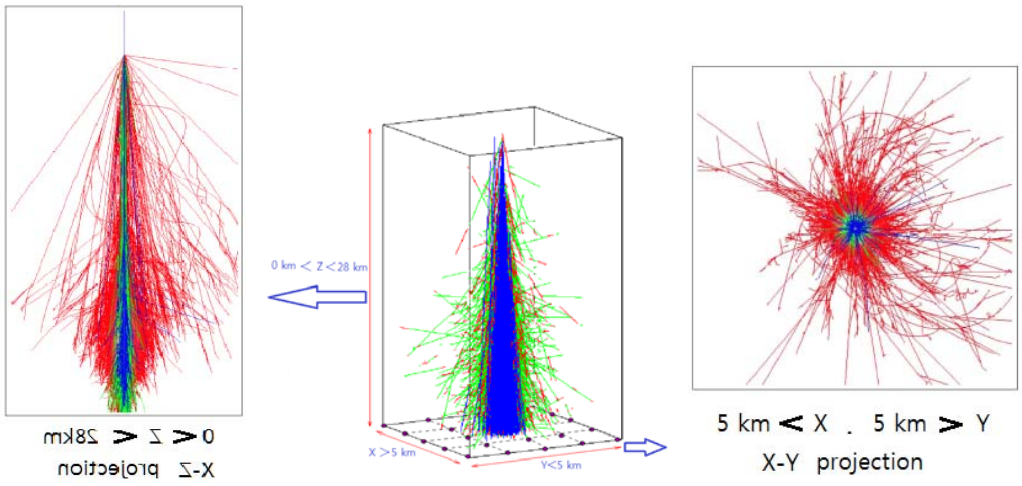

Iron-induced air shower at $\mathbf{E = 1 \times 10^{13} eV}$, $\mathbf{\theta = 0^0}$

Figure 25-25

According to the CORSIKA air shower simulation as Figure 25-25-C total area of X-Y explain at $E = 1 \times 10^{13} eV$ is

$$A_{simulation} = (5km < X)(5km > Y) = 25km^2 \qquad 25\text{-}52$$

According Eq.25-51 by P. Farinella, L.Foschini, Ch. Froeschl, R. Gonczi , T.J.Jopek ,G.Longo and P.Michel Tunguska explosion area is

$$A_{Tunguska} = 2.150 \times 10^3 km^2 \ \pm 50 km^2 \qquad 25\text{-}51$$

difference between Tunguska event areas and Simulation event area on X-Y plain is

$$d_{explosion} = \frac{2150 km^2}{25 km^2} = 86 \qquad 25\text{-}53$$

However, because cosmic ray particle of Tunguska event is accelerated by strongo-magnetic force as stellar force (cf. §8), galactro-magntic force as galactic force(cf.§11) and cosmotro-magnetic force as cosmic force (cf.§13), energy of Tunguska cosmic ray particle should be stronger than electromagnetic energy of CORSIKA air shower simulation as much as

$E_{Tunguska\ cosmic\ ray\ particle} = (1 \times 10^{13} eV)\ (1.190208 \times 10^{7})^{3}$ (86)

$$= 1.449997 \times 10^{36} eV \qquad 25\text{-}54$$

difference by gravitational permittivity of Earth $x_{Earth} = 1.073176$ (cf.§10), gravitational permittivity of air by correspondence number $C_c = 1.5$ (cf.§24), $x_{1.5} = 1.025161$ and electrical permittivity difference of air by correspondence number $C_c = 1.5$ with three forces $(1.5)^3 = 3.375$

$$Q = 0.000589 \times 3.375 = 0.001988,\ x_e = 1.001988 \qquad 25\text{-}55$$

Effective gravitational permittivity of correspondence number by electrical permittivity of air is

$$x_g = \frac{1.025161}{1.001988} = 1.023127 \qquad 25\text{-}56$$

Therefore, net Earth's gravitational permittivity by difference of correspondence number is

$$x_{Earth} = \frac{1.073176}{1.023127} = 1.048918 \qquad 25\text{-}57$$

Therefore, real energy value of primary Tunguska cosmic ray particle is

$$E_{tunguska\ particle} = \frac{1.449997 \times 10^{36}}{1.048918} = 1.382374 \times 10^{36} eV \qquad 25\text{-}58$$

This energy is none other than energy of cosmotomic proton according to Eq.25-46.

$$\gamma_{ACN} = 1.38 \times 10^{36} eV \qquad 25\text{-}46$$

TNT equivalent energy of Hiroshima atom bomb explosion is

$$E_{Hiroshima} = 5.25 \times 10^{32} eV = 20Kt \quad 25\text{-}59$$

Therefore, TNT equivalent energy of Tunguska cosmic ray explosion is

$$E_{Tunguska} = \left(\frac{1.38 \times 10^{36} eV}{5.25 \times 10^{32} eV}\right)(20Kt)$$

$$= (2630)(20Kt) = 52.6\ Mt \quad 25\text{-}60$$

Estimated energy value of Tunguska is $E_{extimated} = 10 - 15\ Mt$(Hunt 1960; Ben& $Menahem$ 1975) and related parameter of height is $h = 7.5\ km$ (Bronshten & Boyarkina, 1971) or $h =$ 8.5km (Ben&Menahem, 1975)

Mean value is

$$h_{mean} = 8 \text{ km} \quad 25\text{-}61$$

Surprisingly, this value is same height of homogeneous atmosphere.

This means that total amount of experienced atmosphere with surface air density for any meteor must be constant (they should be experienced same total air mass and same homogeneous atmosphere regardless a drift direction and an azimuth), despite Earth's atmosphere speared over 1000km.

However, possible air shower height of Tunguska is $h <$ 28km according to the CORSIKA simulation as Figure25-25.

Therefore, we can estimate possible explosion energy range of Tunguska. That is

$$E_{extimated} = (10 - 15\ Mt)\left(\frac{< 28km}{8km}\right)$$

$$= (35 - 52.5\ Mt) <_{h<28km} \quad 25\text{-}62$$

This result means when height reach $\mathrm{h} = 28\mathrm{km}$, limiting value of energy become $E_{limit} = 52.5\ Mt$

Predicted value by CFLE theory is

$$E_{Tunguska} = \left(\frac{1.38 \times 10^{36} eV}{5.25 \times 10^{32} eV}\right)(20Kt)$$

$$= (2630)(20Kt) = 52.6\, Mt \qquad 25\text{-}60$$

Here, we can find good agreement between two values surprisingly that come from very different research field.

Such agreement between two value means that researchers of two different field worked correctly and successfully.

The Tunguska explosion and related anomalies say us that essence of this event is super ultrahigh energy cosmic ray with energy of $1.38 \times 10^{36} eV$ of one proton.

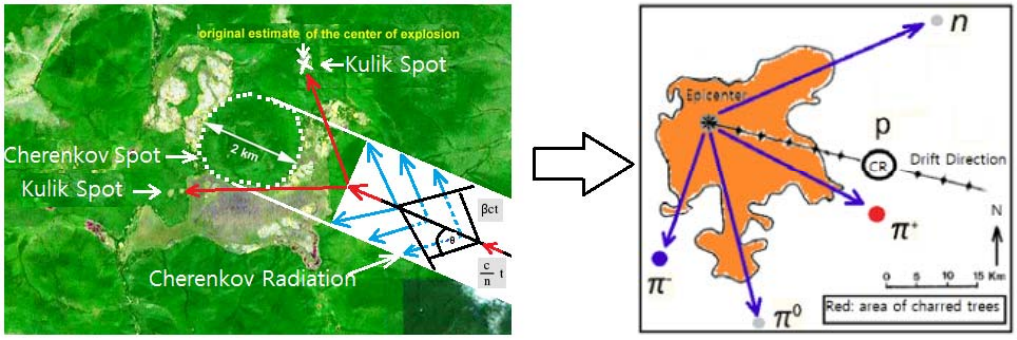

A B

Figure 25-31

Therefore, according to Figure 25-31 we can accept that the ground of Tunguska event is very expensive Russian cosmic ray observatory of important natural surface array in the world. This means that Tunguska site is needed protect for important research.

We need precise and synthetic research (cosmological, astrophysical, geochemical, biological, nuclear physical, medical, ecological ...etc.) about all of the Tunguska phenomena, because Tunguska super explosion is not last blast (probably next one at the great metropolitan city. However, we are not interested such scenario.)

All of such successful consistent explanations about all known anomalies of Tunguska explosion that's cause is only one energetic proton as primary cosmic ray are results of calculable curve of force lines as general relativity of CFLE theory.

25.8. Solving Dimensionless Gravitational Coupling Constant Problem: Why Is the Gravitational Coupling Constant So Weak?

Because so far calculable curve of force lines as general relativity of CFLE theory is very successful, we can expect that to calculate dimensions less gravitational coupling constant by CFLE theory is possible as below.

Original form of pure dimensionless fine structure constant α_e is constituted by possible maximal degree of curve of force line from flat state $g_{flat} = 1$ to $g_{max} = 8$ and change of curve of force line of $g_{accel} = 1.5$ by accelerating universe as

$$\alpha_e = \frac{1}{g_e \times g_e \times C_c \times C_c} = \frac{1}{8 \times 8 \times 1.5 \times 1.5} = \frac{1}{144}$$

$$\rightarrow \frac{1}{144 \cdot x_e} = \frac{1}{137.035999} \text{ (cf. §6)} \qquad 25\text{-}63$$

$\alpha_s = 1$ is strength of the coupling constant for the strong force.

This strength of constant $\alpha_s = 1$ means that flat electric force line is curved more and more from $g_e = 1$ to $g_e = 8$ and interacted with particle of flat strong force line at $g_{strong} = 1$.

α_G is typically defined in terms of the gravitational attraction between pair of electrons. More precisely,

$$\alpha_G = \frac{Gm_e^2}{\hbar c} = \left(\frac{m_e}{m_P}\right)^2 \approx 1.7518 \times 10^{-45} \qquad 25\text{-}64$$

where G is the gravitational constant, m_e is the electron rest mass, c is the speed of light in vacuum, $\hbar$ is the reduced Planck constant, m_p is the Planck mass.

However, by charge interval constant $\mathrm{N} = 1.686044 \times 10^{21}$from §3.3 in CFLE theory this dimensions less gravitational coupling constant can be calculated as

$$N = \frac{1}{1.686044 \times 10^{21}} = 5.931043 \times 10^{-22} \quad \text{25-65}$$

Force interval constant form §3.3 in CFLE theory is

$$N^2 = 3.517727 \times 10^{-43} \quad \text{25-66}$$

Because frame of reference is $\alpha_s = 1 = \frac{137.035999}{137.035999} = \frac{137.035999}{(8 \times 1.5 \times 8 \times 1.5)(x_i)}$ and related curve of force line of Earth $(f_K)^2 = (1.202)^2(1.007068)^2 = 1.465230$ (cf. §5, §11) is, Difference for gravitational coupling constant on Earth at $\mathrm{g} = 1$ is

$$d_{\alpha_s} = 137.035999,\ d_{C_c} = 1.465230 \quad \text{25-67}$$

where 1.007068 is difference by electrical permittivity of air at $\mathrm{g}.\ C_c = (8)(1.5) = 12 \rightarrow \mathrm{Q} = (12)(0.000589) = 0.007068 \rightarrow x_{e.air} = 1.007068$(cf.§6,§10).

Therefore, predicted value by dimensionless constant of N, g from CFLE theory is

$$\alpha_G = \frac{3.517727 \times 10^{-43}}{(137.035999)(1.465)} = 1.752 \times 10^{-45} \quad \text{25-68}$$

Calculating value by dimension of $\mathrm{G}, m_e, m_p, c, \hbar\ of$ Eq.25-64 is

$$\alpha_G = \frac{G m_e^2}{\hbar c} = \left(\frac{m_e}{m_{Planck}}\right)^2 \approx 1.7518 \times 10^{-45} \quad \text{25-64}$$

Two values agree very well.

Therefore, we can say that CFLE theory can calculate the dimensionless physical constants.

Because massive seed of elementary particle (cf. §3, §4) is screened by three kind of force lines (strongomagnetic, electromagnetic and weakomagnetic), gravitational charge (Newtonian rest mass) and related coupling constant is appeared so weak.

25.9. Solving the Large-Scale Anisotropy Problem: Is the Universe at Very Large Scales Anisotropic, Making the Cosmological Principle an Invalid Assumption?

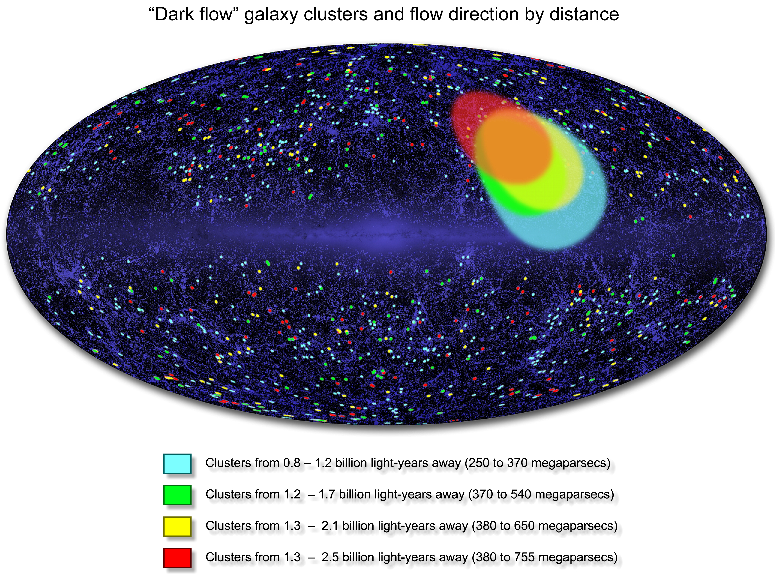

Figure 25-34

By existence of correspondence number $C_c = 1.5$ from accelerating universe it is expected mass center of the universe as cosmic nucleus as mentioned§13 and §24.

Because cosmic nucleus exist, must be appeared that the motion of galaxy clusters with respect to the cosmic microwave background should not be randomly distributed in all directions as so called dark flow (cf.§24) as Figure 25-34 and Figure 25-35 against to standard cosmological models.

Such motion of dark flow to explain is very simple in CFLE theory.
In Earth's magnetic field from Earth's gravitational charge (Earth's mass) electrically charged particle traps and move. Figure 25-35 show moving charged particles in Earth's magnetic field.

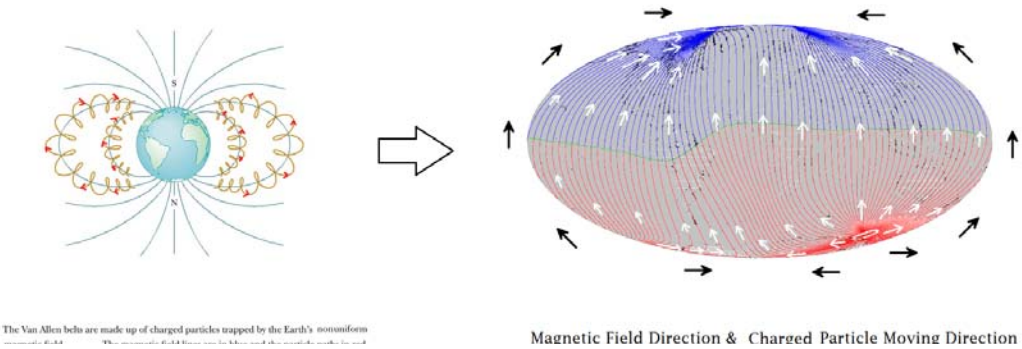

Figure 25-35

Figure 25-36-A is depicted magnetic field of mass center of universe (right side) and 25-36-B is observed direction of motion of galaxy clusters by A. Kashlinsky.

Observed result can explain simply according to CFLE theory that galaxy cluster moving along cosmic magnetic force line from mass center of universe.

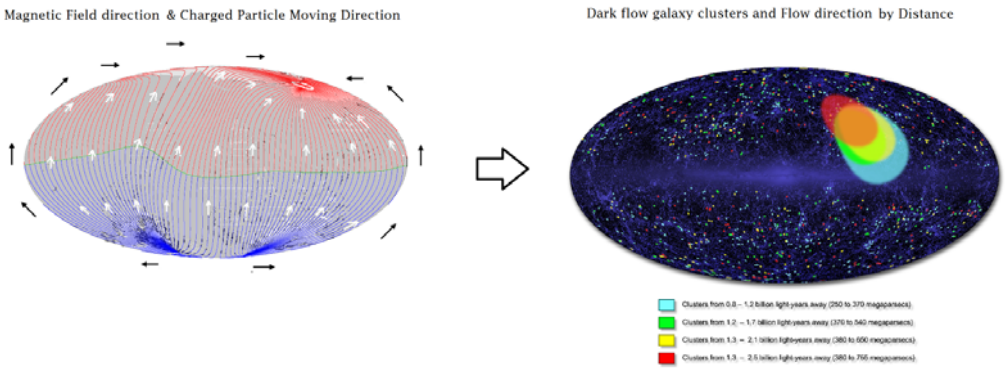

A **B**

Figure 25-36

Because mass center of the universe exist, other features of large-scale anisotropy which are not consistent with the modern Big Bang model with Einstein's general relativity and cosmological principle should be observed.

Surprisingly, there are such observation's results in Radio Astronomy and High Energy Cosmic Ray.

The number count and intensity dipole anisotropy in radio, NRAO VLA Sky Survey (National Radio Astronomy Observatory Very Large Array Sky Survey or NVSS) catalogue is inconsistent with the local motion as derived from cosmic microwave background and indicate intrinsic dipole anisotropy (cf. J J Condon, W D Cotton, E W Greisen, Q F Yin, R. A. Perley, G. B. Taylor, and J J Broderick."The NRAO VLA Sky Survey"AJ, 115(5):1693-1716, May 1998, A. K. Singal. "Large Peculiar Motion of the Solar System from the Dipole Anisotropy in Sky Brightness due to Distant Radio Sources."ApJL, 742:L23, December 2011, Prabhakar Tiwari, Rahul Kothari, Abhishek Naskar, Sharvari Nadkarni-Ghosh, Pankaj Jain. "Dipole anisotropy in sky brightness and source count distribution in radio NVSS data")

The same NVSS radio data also shows an intrinsic dipole in polarization density and degree of polarization in the same direction as in number count and intensity. (cf.Prabhakar Tiwari and Pankaj Jain. "Dipole anisotropy in integrated linearly polarized flux density in NVSS data)

There are other several observation revealing large-scale anisotropy.

The optical polarization from quasars shows polarization alignment over a very large scale of Gpc.

(cf. Pankaj Jain, Gaurav Narain, and S Sarala. "Large-scale alignment of optical polarizations from distant QSOs using coordinate-invariant statistics."MNRAS, 347(2):394-402, 2004.).

The cosmic-microwave-background data shows several features of anisotropy, which are not consistent with the Big Bang model too (cf. H.K. Eriksen, F.K. Hansen, A.J. Banday, K.M. Gorski, and P.B. Lilje. "Asymmetries in the Cosmic Microwave Background anisotropy field."ApJ, 605:14–20, 2004, Pramoda Kumar Samal, Rajib Saha, Pankaj Jain, and John P. Ralston."Signals of Statistical Anisotropy in WMAP Foreground-Cleaned Maps."MNRAS, 396:511, 2009).

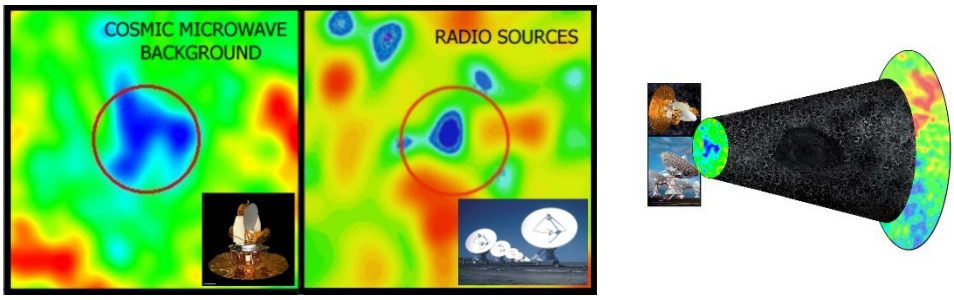

Figure 25-37

NVSS team have found an enormous hole in the Universe, nearly a billion light-years across, empty of both normal matter such as stars, galaxies, and gas, and the mysterious, unseen "dark matter." While earlier studies have shown holes, or voids, in the large-scale structure of the Universe. "Not only has no one ever found a void this big, but we never even expected to find one this size," said Lawrence Rudnick of the University of Minnesota. Astronomers have known for years that, on large scales, the Universe has voids largely empty of matter. However, most of these voids are much smaller than the one found by Rudnick and his colleagues. In addition, the number of discovered voids decreases as the size increases.

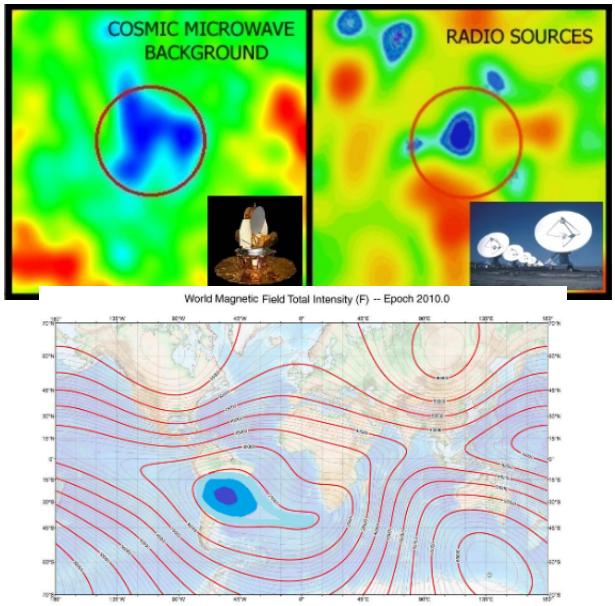

Figure 25-38

In CFLE theory such an enormous hole in the Universe can be explained by cosmic magnetic hole that result of cosmic magnetic interaction between rotation magnet of cosmic mass center and orbital magnet of total universe as Earth's magnetic hole so called South Atlantic Anomaly(SAA) that is the near-Earth region where the Earth's magnetic field is weakest relative to an idealized Earth-centered dipole field. (cf. §15: magnetic interaction between spin magnet of Earth and orbital magnet of Earth).

The South Atlantic Anomaly (right side of Figure 25-38) is an area where the Earth's inner Van Allen radiation belt comes closest to the Earth's surface dipping down to an altitude of 200 km above sky of Brazil.

This leads to an increased flux of energetic particles in this region and exposes orbiting satellites to higher-than-usual levels of radiation (cf. §15).

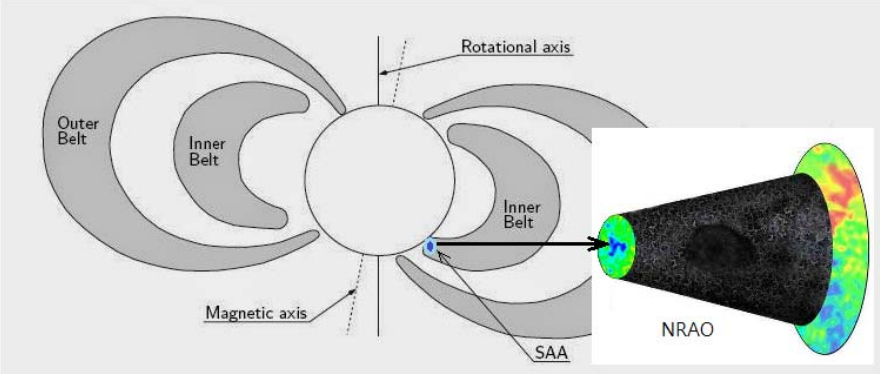

Third Van Allen belt is omitted

Figure 25-39

In Figure 25-39 magnetic hole of SAA correspond an enormous cosmic hole that was founded by NARO team of Lawrence Rudnick of the University of Minnesota. Without inner magnetic source as cosmic mass center cannot be imaging such huge hole system of universe as Figure 25-39.

Therefore, large scale anisotropy in the arrival direction of high energetic cosmic rays detected above energy of 10^{21}eV is expected by cosmotomic nucleus as Figure 25-40-B

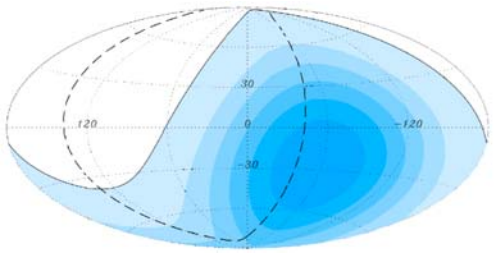

Darker color means a higher exposure.

Figure 25-40-B

Figure 25-40-A show that solar mass ejection of period of solar activity. Here, important point is that energy isotropy around the active sun is broken.
If cosmotomic nucleus were activated as the sun, energy isotropy around active cosmic mass center could be broken as Figure 25-40-B.

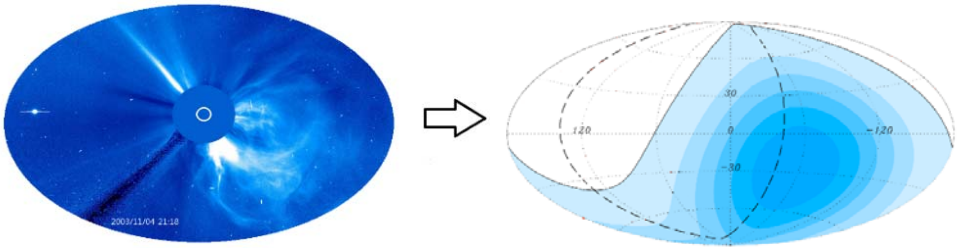

A **B**

Figure 25-40

However, after activity of the cosmotomic nucleus such energy anisotropy could be remained as Figure 25-40-B.
Therefore, extra galactic cosmic rays that accelerated by curved galactic field with $E_{\gamma AGN} = 3.05 \times 10^{21} eV$ (Eq.25-44) from cosmic mass center should be distributed Figure 25-40-B because of strong remained energy from cosmotomic activity.

Because observation possibility of such ultra-high energy cosmic ray like Tunguska cosmic ray must be very lower than knee cosmic ray (1 particle $/m^2/year$) and ankle cosmic ray (1 particle/$km^2/year$), we should be needed long time observation for large scale cosmic ray anisotropy to obtain or very large cosmic ray space observatory(VLCRSO) like AMS 2.

Despite such difficulty, using data collected at the Pierre Auger Observatory during the past 3.7 years, scientists (444 authors in Pierre Auger collaboration: J. Abraham et al.) demonstrated a correlation between the arrival directions of cosmic rays with energy above $\sim 6 \times 10^{19}$eV and the positions of active galactic nuclei (AGN) lying within ~75 mega parsecs. They rejected the hypothesis of an isotropic distribution of these cosmic rays with at least a 99% confidence level from a prescribed a priori test. The correlation they observed is compatible with the hypothesis that the highest energy particles originate from nearby extragalactic sources whose flux has not been substantially reduced by interaction with the cosmic background radiation. AGN or objects having a similar spatial distribution are possible sources.

(However, in ArXive:1409.3128v1.10 Sep 2014 is it reported by Pierre Auger Observatory and the Telescope Array: The resulting multipolar expansion of the flux of cosmic rays allows us to perform a series of anisotropy searches, and in particular to report on the angular power spectrum of cosmic rays above 10^{19}eV . No significant deviation from isotropic expectations is found throughout the analyses performed.)

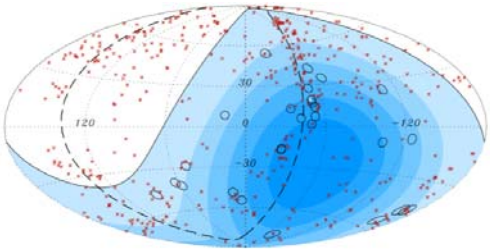

Aitoff projection of the celestial sphere in galactic coordinates with circles of radius3:1 centered at the arrival directions of the 27 cosmic rays with highest energy detected by the Pierre Auger Observatory. The positions of the 472 AGN (318 in the field of view of the Observatory) with redshift $z \leq 0.018$ (D < 75 Mpc) from the 12th edition of the catalog of quasars and active nuclei are indicated by red asterisks. The solid line represents the border of the field of view (zenith angles smaller than 60^o). Darker color indicates larger relative exposure. Each colored band has equal integrated exposure. The dashed line is the super galactic plane. Centaurus A, one of our closest AGN, is marked in white from arXive: 0722.2256v1 [astro-ph] 14 Nov 2007

Figure 25-41

Furthermore, present observation summary of IceCube Neutrino observatory at the Amundsen–Scott South Pole Station in Antarctica are

●IceCube records several 10^{10} cosmic ray events per year. This allows for a study of anisotropies in the *cosmic ray arrival direction distribution* in the southern hemisphere at the part-per-mille level and less.

●IceCube sees a *large-scale anisotropy* in cosmic ray arrival directions in the southern sky.

●The IceCube sky map also shows a broad (~20°) excess region around right ascension 120°, with an equally strong deficit around right ascension 220°.

●Similar anisotropies have been observed by experiments in the northern hemisphere

●The origin of these anisotropies is currently not known. In the near future, IceCube can study whether the anisotropy persists at higher energy (>100 TeV).

●Soon, they will have full sky coverage with IceCube (south) and HAWC (north).

Conclusion of Milagro collaboration are

● Large-Scale Anisotropy firmly established

- Observed by a number of experiments including Milagro

- Suggestions of time dependence

● Localized anisotropy at 5×10^{-4} level

- No compelling explanation.

- Non-standard cosmic-ray diffusion

● Cosmic Ray Anisotropy may be quite revealing

Therefore, such summary about anisotropy we can be analyzed by general relativity of CFLE theory that cosmotomic nucleus exist in the universe as proton in hydrogen atom according to Figure 25-39 and 25-40.

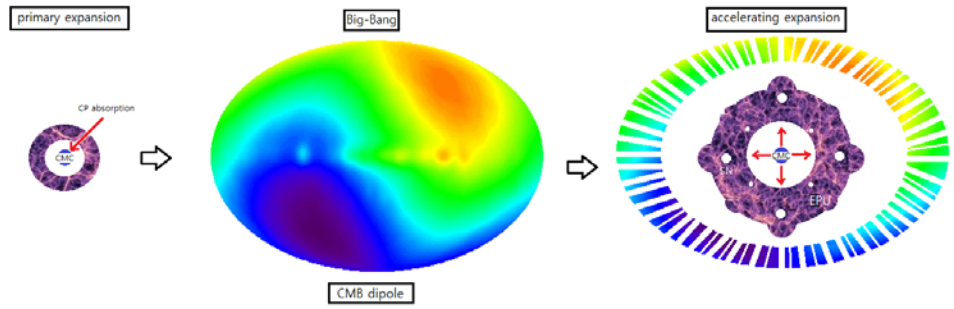

Figure 25-42

Figure 25-42-A show primary expansion of the universe between Cosmic Mass Center (CMC) and Part of Expansion of Universe (EPU) by cosmic photon absorption as emitting electron from neutron decay. Here, Cosmic Photon (CP) is end product of annihilation of the universe (cf. §13, §24). Figure 25-42-B show normal Big-Bang of EPU. Figure 25-42-C show accelerating expansion of EPU. Because during expansion stellar neutrons (SN: white dots) are synthesis as stellar helium, expansion of EPU is accelerated (expressed convex) (cf. §24).

Therefore, we can conclude that because of anisotropy of the universe by cosmic mass center, cosmological principle (or Copernican principle) is wrong assumption. Because of existence of cosmic mass center instead black hole and related singularity, standard big bang model by curved space-time continuum, related string theory and multi verse is wrong.